J. Fluid Mech. (1980), *vol.* 98, *part* 3, *pp.* 473–508
Printed in Great Britain

The effect of finite turbulence spatial scale on the amplification of turbulence by a contracting stream

By M. E. GOLDSTEIN

National Aeronautics and Space Administration,
Lewis Research Center, Cleveland, Ohio 44135

AND P. A. DURBIN

Department of Applied Mathematics and Theoretical Physics,
University of Cambridge, Silver Street, Cambridge CB3 9EW

(Received 13 April 1979 and in revised form 4 October 1979)

An alternative to Hunt's (1973) extension of classical rapid distortion theory is used to calculate the turbulence downstream of a rapid contraction. This problem was originally studied by Batchelor & Proudman (1954) and Ribner & Tucker (1953), but their analyses were restricted to flows in which the characteristic turbulence scales were small compared to the spatial scales of the mean flow (usually the characteristic dimension of the apparatus). We now consider the case where the turbulence scale can have the same magnitude as the mean-flow spatial scale. Relatively simple formulae are obtained by calculating the turbulence only in the downstream region where the mean flow is no longer affected by the potential field of the contraction.

The results are then further simplified by assuming that the contraction is large and expanding in inverse powers of the contraction ratio. The calculations show that effects of finite turbulence scale can be quite significant. We also obtain some important new results for small-scale turbulence by expanding the solutions in inverse powers of the turbulence spatial scale.

1. Introduction

It is now believed that large-scale atmospheric turbulence drawn into the inlet is the major cause of aircraft-engine tone noise when the airplane is on the ground and has only small forward velocity. These tones are generated because the contraction of the flow into the inlet causes the turbulent eddies to elongate in the streamwise direction while causing their transverse velocities to be amplified. Then the fan blades can cut through a coherent eddy structure many times before it leaves the blade row and the eddy therefore acts like a steady inlet flow distortion which is known to produce a pure tone sound field at the blade-passing frequency of the fan (Goldstein 1976, pp. 175–208). There is considerable interest in predicting the tones produced by this inlet–turbulence interaction and in order to do this it is necessary to know the structure of the turbulence at the fan face.

Free-stream turbulence is, on the other hand, known to have an important effect on boundary-layer separation and transition and there has recently been considerable

0022-1120/80/4451-1050 $02.00

interest in predicting this effect – especially in the turbine and compressor stages of gas turbine engines where there can be large amounts of turbulence in the stream. In order to do this we must know the turbulence structure at the edge of the critical region of the boundary layer, which, in turbine stages, is often downstream of a very large contraction.

In both these cases it is necessary to calculate the turbulence in a stream that has undergone a large contraction from an upstream state where the turbulence is more or less isotropic. (In the latter case the severe contractions are encountered for the most part only in the turbine stages.) Needless to say, such calculations are also of interest in their own right. Until recently, these calculations could only be performed by using the classical rapid distortion theory initiated by Taylor (1935) and developed by Batchelor & Proudman (1954) and Ribner & Tucker (1953). This theory leads to very simple results but involves the assumption that the spatial scale of the turbulence is small relative to the spatial scale of the mean-flow velocity gradients. It also involves the assumption that the turbulence intensity be much less than the ratio of these two scales and therefore that the turbulence be very weak indeed.

However, Hunt (1973) has now developed extension of the theory that applies even when the turbulence spatial scale is of the order of or larger than the scale of the mean flow velocity gradients – in which case the restriction on the magnitude of the turbulence intensity is much less severe.

By using careful dimensional reasoning, Hunt showed that turbulent fluctuations are governed by the inviscid momentum and continuity equations linearized about an appropriate steady potential flow. He considered only the case where the Mach number is zero and the mean flow is two-dimensional. With these restrictions he was able to obtain the required solutions to the linearized equations by first using Cauchy's formula linearized about the mean flow (Batchelor 1967, p. 276) to determine the vorticity perturbations and then using the latter to calculate the vortical part of the velocity field. This last step was accomplished by solving three second-order partial differential equations. The non-vortical part of the velocity was then determined by solving a fourth partial differential equation.

A few years later, Goldstein (1978, 1979) showed that the most general vortical and entropic, compressible or incompressible, steady or unsteady solution to the inviscid momentum and continuity equations linearized about a steady compressible or incompressible potential flow (which can be either two- or three-dimensional) can be found by solving a *single* second-order partial differential equation, whose solution is associated with the non-vortical part of the velocity field. In Goldstein's approach the vortical part of the velocity field is *given* and there is no need to calculate it from the vorticity. This result is based on a decomposition of the velocity field into an irrotational part that is associated with the pressure fluctuations and a rotational part that carries all the vorticity and is completely independent of the pressure fluctuations. The vortical part is a known function of the upstream boundary conditions and the mean potential flow and only the irrotational part (which can be expressed in terms of a scalar potential) need ever be calculated.

Random upstream entropy (or temperature) fluctuations can produce additional turbulence downstream of a contraction (Goldstein 1979). This effect is especially important in the application of the theory to the turbine-stage problem that was described above. But, even though the approach of this paper, which is based on

Goldstein's (1978) theory, can easily be generalized to deal with this effect, we shall not do so here. The interested reader is referred to Goldstein (1979) for a discussion of the high-frequency solutions to this problem.

The formulation given by Goldstein (1978) is simpler than the one used by Hunt, even for the incompressible two-dimensional mean flow that he treated. But, even with this simplification, a great increase in complexity is incurred when the classical restriction of small turbulence length scale is removed. However, the present analysis can be considerably simplified by first assuming that the mean flow becomes parallel at downstream infinity and then calculating the turbulence far enough downstream from the contraction to ensure that the non-uniformity of the mean flow field has decayed. The turbulence then acts like a small perturbation on a *uniform* flow and therefore has a considerably simplified structure. But, even though we are able to obtain relatively simple analytical solutions to this problem, they still lead to rather complex formulas for the experimentally interesting statistical properties of the turbulence. These quantities can therefore not be determined without a considerable amount of numerical computations.

However, for applications such as those described above we are usually interested in large contractions and in this paper we shall simplify the formulae by treating the inverse contraction ratio as a small parameter (rather than by invoking the classical restriction on the turbulence scale). We expect our results to apply even when the contraction ratio is not too large, since the large contraction ratio asymptotic expansion of the classical rapid-distortion theory results agree with the general formulae even for moderate contractions (Batchelor & Proudman 1954).

We can interpret the present results as corrections to classical rapid-distortion theory that account for effects due to the finiteness of the turbulent spatial scale. They include wall-backage effects and the effects of non-uniform mean strains on the distortions of the upstream turbulence by the mean velocity field. The numerical calculations show that these effects can change the mean-square turbulence velocity by more than a factor of two even when the turbulence scale is as small as the transverse dimension of the downstream channel.

In § 2 we discuss the physical model and the linearized equations that govern the turbulence motion. The statistical concepts that relate the solutions of these equations to the turbulence correlations are described in § 3. The equations are then solved in the region downstream of the contraction in § 4 (without imposing *any* restrictions on the magnitude of the contraction ratio or the scale of the turbulence).

The upstream flow can be an external stream, such as would occur for the flow into an inlet, or it can be an internal flow of larger cross-section. Some typical configurations are shown in figure 2.

The large contraction ratio limit is treated in § 5 and appropriate limiting forms of the solutions of § 2 are obtained by using the method of stationary phase (Erdélyi 1956). The simplified formulas are then used to calculate turbulence intensities and one-dimensional spectra in the region downstream of the contraction.

The classical rapid-distortion theory limit is considered in § 6 and results are obtained for arbitrary contraction ratio by transforming a formula given by Batchelor & Proudman (1954) into an appropriate co-ordinate system. The transformation is different at each point of the flow and depends on the geometry of the contraction.

The numerical results and their physical implications are discussed in § 7. They show

that the amplification effect of the contraction is reduced when the spatial scale of the turbulence increases. In fact, the upstream turbulence is actually suppressed when the contraction ratio is less than 5 and the turbulence spatial scale is larger than three times the transverse dimensions of the downstream channel.

2. The governing equations and basic assumptions

Rapid-distortion theory of turbulence was originated by Taylor (1935) who suggested that the turbulent vorticity be determined first and that the turbulent velocity then be calculated from this quantity. This approach was followed by Hunt (1973) who generalized the theory to include large-scale turbulence. However, Goldstein's (1978) approach, which we shall follow here, determines the vortical part of the velocity field directly and does not require that it be calculated from the vorticity.

We shall consider a high Reynolds number turbulent flow that passes through a contraction and has a uniform mean velocity at upstream infinity. We then assume, as is usual in rapid distortions theory, that:

(i) the upstream turbulence is weak, i.e. the upstream turbulence intensity u'_∞/U_∞ (where u'_∞ is a typical r.m.s. turbulence velocity and U_∞ is the upstream mean flow velocity) is much less than one;

(ii) the distortion of turbulent vortex lines by mean straining is much greater than that produced by turbulent straining;

(iii) the mean flow and turbulence Reynolds numbers are both large;

(iv) the flow is unseparated and the turbulence spatial scale is large compared with the boundary-layer thickness.

These assumptions are sufficient to ensure that the turbulence can, in the main, be calculated from inviscid equations linearized about a steady mean flow, which can be taken as the potential flow through the contraction. However, they do not ensure that the linearized equations will be valid at all points of the flow. But, in most cases, this only causes the solutions to 'break down' in some limited regions of the flow.

Consider, for example, a weakly turbulent flow into an inlet with width δ. The situation is then similar to the one depicted in figure 2(*c*). It is known that linearized theory becomes invalid within a certain distance s of the stagnation point, A. This distance is small compared to the characteristic dimension, a, of the external flow, i.e.

$$s/a = \epsilon \ll 1.$$

Now, owing to the contraction of the mean-flow stream tubes, a streamline that enters the inlet after passing within a distance s of the stagnation point will lie within a distance $O(\delta s/a)$ of the channel wall once it has passed downstream of the inlet. (It may be helpful here to think of the case where $\delta/a \ll 1$.) Then, the turbulence that enters the inlet after passing within a distance $O(a\epsilon)$ of the stagnation point is confined to a wall layer of thickness

$$\delta_w/\delta = \epsilon.$$

We expect the linearized equations to be invalid within this region, which is in any case always much thinner than the width of the downstream channel.

As long as condition (iv) is satisfied, the appropriate boundary conditions at the solid surfaces surrounding the flow is that the normal component of the turbulence

velocity vanish at these surfaces. It is well known that we can apply this boundary condition directly to the solutions of the inviscid equations even though these equations are invalid near the surface.

In a similar vein, we can impose this surface boundary condition on the solution to the linearized equations even though these equations are invalid within a distance of $O(\delta_w)$ from the wall.

We also expect the linearized analysis to become invalid in any region that is far enough downstream from the contraction so that the time $d/(U_\infty a/\delta)$ (where d is a typical distance between this region and the contraction; the end of the contraction being where the mean flow is deemed essentially uniform) it takes a fluid particle to reach this region is no longer small compared to the time scale l_∞/u'_∞ on which non-linear interactions occur. That is, in any region for which

$$(u'_\infty \delta/U_\infty a)\, d/l_\infty = O(1).$$

(The same restriction applies to the distance between the upstream turbulence source and the contraction. However, the turbulence will be approximately isotropic upstream of contraction and the well-known corrections for decay can be applied. It might also be desirable to apply such corrections to the complete turbulent flow calculated in the subsequent analysis, cf. Tucker & Reynolds (1968).)

In order to simplify the subsequent analysis we shall ultimately require that the turbulence be calculated in a region that is far enough downstream from the contraction to ensure that its statistical properties have become uniform in the flow direction. Since this region lies within a few integral scales of the contraction, the preceding equality is easily satisfied.

It is probably not necessary to require that condition (iv) hold everywhere in the flow, in that the boundary layer can be allowed to separate if it then reattaches at a point that is not too far downstream. In order to ensure that this requirement be met for inlet flows involving large contractions we may have to suppose that some form of boundary-layer control (e.g. suction) is imposed at the inlet lip.

When the contraction lies within a continuous duct, such as the ones depicted in figures 2(*a*) and (*b*), the wall boundary layers could become turbulent if the mainstream turbulence were produced by a 'turbulence generator' which was located sufficiently far upstream of the contraction. We will then have to assume that the weak irrotational flow which these boundary layers induce in the mainstream (Phillips 1955) is everywhere small compared to the mainstream turbulence fluctuations in the region downstream of the contraction where we shall ultimately calculate them.

On the other hand the large contractions with which we are mainly concerned will tend to relaminarize the boundary layers and thereby minimize these irrotational fluctuations.

When the above requirements are met it should be possible to calculate the mainstream turbulence from the inviscid equations of continuity and momentum linearized about the steady potential flow that corresponds to the particular contraction being considered. Thus, we can write the velocity $\mathbf{v}$ and pressure p as

$$\mathbf{v} = \mathbf{U}(\mathbf{x}) + \mathbf{u}(\mathbf{x}, t),$$

$$p = P(\mathbf{x}) + p'(\mathbf{x}, t),$$

where $\mathbf{U}$ and P are the velocity and pressure of the steady potential flow through the contraction and $\mathbf{u}(\mathbf{x},t)$ and p' are the velocity and pressure fluctuations of the turbulence. The latter quantities are solutions to the linearized equations alluded to above.

Goldstein (1978) showed that it follows from the form of these equations that the velocity perturbation $\mathbf{u}$ has the decomposition

$$\mathbf{u} = \nabla\phi + \mathbf{u}^{(I)}, \tag{2.1}$$

where the irrotational contribution $\nabla\phi$ is related to the pressure fluctuations p' by

$$p'/\rho_0 = -D_0\phi/Dt. \tag{2.2}$$

Here, $D_0/Dt \equiv \partial/\partial t + \mathbf{U}.\nabla$ is the convective derivative based on the mean flow velocity $\mathbf{U} = \{U_1, U_2, U_3\}$, ρ_0 is the mean-flow density and t denotes the time. The contribution $\mathbf{u}^{(I)}$ carries the vorticity and is independent of the pressure fluctuations; but, even more importantly, is completely known in terms of the mean-flow quantities and the upstream boundary conditions. For the homentropic (i.e., constant entropy) flow to which we shall restrict the present analysis, $\mathbf{u}^{(I)} = \{u_1^{(I)}, u_2^{(I)}, u_3^{(I)}\}$ is given by

$$u_i^{(I)} = \mathbf{u}_\infty(\mathbf{X} - \hat{\mathbf{1}}U_\infty t).\partial\mathbf{X}/\partial x_i \quad \text{for} \quad i = 1, 2, 3, \tag{2.3}$$

where $\mathbf{u}_\infty$ is the upstream velocity perturbation which has zero divergence, produces no pressure fluctuations and is effectively frozen in the flow. It can be specified as an upstream boundary condition in any given problem and can therefore be considered to be known. It is discussed at greater length near the end of this section. The quantity $\hat{\mathbf{1}}$ denotes a unit vector in the x_1 direction and U_∞ denotes the constant upstream mean-flow velocity (which is assumed to be in this direction). $\mathbf{u}^{(I)}$ depends on the mean flow through the vector function $\mathbf{X} = \{X_1, X_2, X_3\}$ of the position co-ordinate vector $\mathbf{x} = \{x_1, x_2, x_3\}$. The vector $\mathbf{X} - \hat{\mathbf{1}}U_\infty t$ represents the Lagrangian co-ordinates of a fluid particle that originated at upstream infinity at a position with transverse co-ordinates $x_2 = X_2$ and $x_3 = X_3$. As this particle moves downstream it travels along the mean-flow streamlines which lie on the intersections of the surfaces $X_2 =$ constant and $X_3 =$ constant as shown in figure 1. Then, provided the mean flow is not a two-dimensional flow with net circulation, $X_2 \to x_2$ and $X_3 \to x_3$ far upstream in the flow (i.e. at $x_1 = -\infty$). The modifications of the theory that are needed to cope with two-dimensional flows with non-zero circulation are discussed by Goldstein (1978).

When the mean flow is two-dimensional we can set

$$X_3 = x_3, \tag{2.4}$$

and

$$X_2 = \Psi/U_\infty, \tag{2.5}$$

where Ψ is the stream function of the mean potential flow.

As long as the mean flow is not a two-dimensional flow with a net source strength at infinity X_1/U_∞ will approach x_1/U_∞ as $x_1 \to -\infty$ and at all other points will equal the Lighthill (1956)–Darwin (1953) 'drift' function

$$\frac{x_1}{U_\infty} + \int_{-\infty}^{x_1} \left[\frac{1}{U_1(x_1', y_s(x_1', X_2, X_3), z_s(x_1', X_2, X_3))} - \frac{1}{U_\infty} \right] dx_1'. \tag{2.6}$$

Here x_1', y_s, z_s are the points of the streamline along which the mean flow fluid particle travels. The change in X_1/U_∞ between any two points on this streamline is equal to

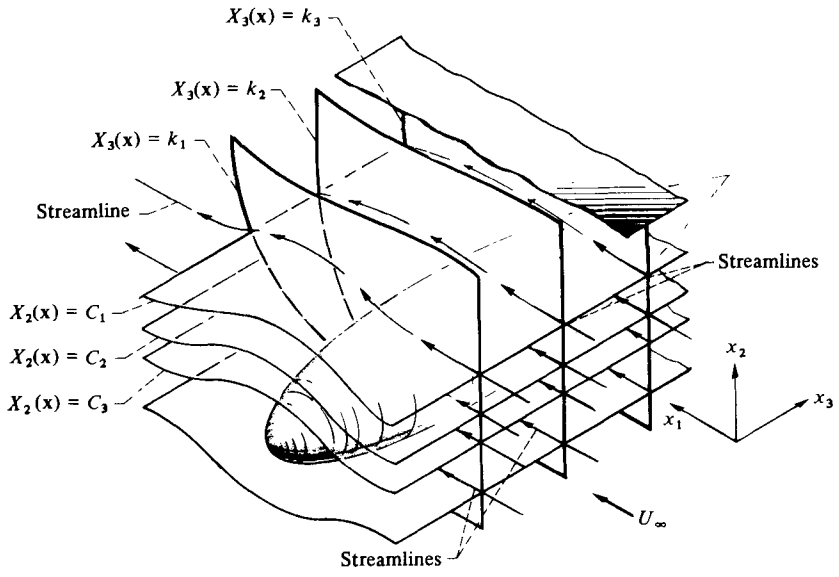

FIGURE 1. Illustration of X_2 and X_3 surfaces.

the time it takes a fluid particle to traverse the distance between those points. Then $X_1 - U_\infty t$ remains constant relative to an observer moving with the mean flow fluid particle and is therefore a Lagrangian co-ordinate for that particle.

In the general case the perturbation potential ϕ is found by solving a linear inhomogeneous scalar wave equation which is obtained by substituting (2.1) and (2.2) into the linearized continuity equation (the linearized momentum equation are satisfied by these formulas for any choice of ϕ). But we shall limit the analysis to incompressible flow, so that the continuity equation requires that $\mathbf{u}$ have zero divergence and therefore that

$$\nabla^2\phi = -\nabla . \mathbf{u}^{(I)}. \tag{2.7}$$

Since $\mathbf{u}^{(I)}$ is known, this equation is to be solved for ϕ subject to the boundary condition

$$\hat{\mathbf{n}} . \nabla\phi = -\hat{\mathbf{n}} . \mathbf{u}^{(I)} \quad \text{on} \quad S, \tag{2.8}$$

that the total velocity in the normal direction $\hat{\mathbf{n}}$ vanish on all solid surfaces S bounding the flow.

As we have already indicated $\mathbf{u}^{(I)}$ becomes equal to the upstream solenoidal (i.e. divergence-free) velocity perturbation $\mathbf{u}_\infty(\mathbf{x} - \hat{\mathbf{i}}U_\infty t)$, at upstream infinity (where the mean flow is uniform). Then the source term in (2.7) will vanish as $x_1 \to -\infty$ and we can require that

$$\phi \to 0 \quad \text{as} \quad x_1 \to -\infty, \tag{2.9}$$

which in view of (2.1) and (2.2) implies that the irrotational part of the velocity field will vanish and there will therefore be no pressure fluctuations at upstream infinity. The entire perturbation velocity will then be equal to $\mathbf{u}_\infty$, i.e.

$$\mathbf{u} \to \mathbf{u}_\infty(\mathbf{x} - \hat{\mathbf{i}}U_\infty t) \quad \text{as} \quad x_1 \to -\infty. \tag{2.10}$$

It is well known (Kovasznay 1953) that the most general small-amplitude notion that can be imposed on a uniform (i.e. constant velocity) flow has a velocity field

that can be decomposed into the sum of (i) a disturbance $\mathbf{u}_\infty(\mathbf{x}-\hat{\mathbf{1}}U_\infty t)$ that is purely convected (i.e. frozen in the flow), has zero divergence and is completely decoupled from the fluctuations in pressure or any other thermodynamic property and (ii) an irrotational disturbance that produces no entropy fluctuations but is directly related to the pressure fluctuations. It is important to notice that each of these modes of motion is itself a solution to the governing equations and can therefore be imposed on the flow independently of the others. In fact, the upstream vortical velocity $\mathbf{u}_\infty(\mathbf{x}-\hat{\mathbf{1}}U_\infty t)$ will satisfy the governing equations for any vector function $\mathbf{u}_\infty$ of the indicated argument, subject only to the requirement that $\nabla.\mathbf{u}_\infty = 0$ (which determines one of the components of $\mathbf{u}_\infty$ in terms of the other two) and perhaps the requirement that $u_{\infty 2} = 0$ at the upstream boundaries when the contraction occurs in a continuous duct. We can therefore specify the function $\mathbf{u}_\infty$ as an upstream boundary condition and the upstream solution will then behave like the small-amplitude vortical motion on a uniform flow.

Now, it is also known that any weak turbulent motion that might be imposed on a uniform mean flow can be represented by this type of vortical velocity field. It is therefore appropriate to impose the upstream condition (2.9) and specify the components of $\mathbf{u}_\infty(\mathbf{x}-\hat{\mathbf{1}}U_\infty t)$ as an upstream boundary condition.

We shall require that the upstream turbulent vorticity be homogeneous. This type of flow can be generated in the laboratory by inserting a 'homogenizing device', such as a wind tunnel grid, into the upstream region. When the contraction takes place within a continuous duct the upstream turbulent velocity will always be non-homogeneous within a wall layer of thickness $O(l_\infty)$. In order to ensure that the vorticity be homogeneous over most of the upstream region we will have to require that the cross-stream dimension a of the upstream duct be much larger than the turbulence scale l_∞. The non-homogeneous wall-layer turbulence should then have a relatively small effect on the downstream flow.

3. Calculation of velocity field due to random homogeneous incident distortion

It is easy to see that the local velocity field due to an upstream harmonic vortical velocity distortion

$$\mathbf{u}_\infty(\mathbf{x}-\hat{\mathbf{1}}U_\infty t) = \hat{\mathbf{u}}^\infty(\mathbf{k})\exp[i\mathbf{k}.(\mathbf{x}-\hat{\mathbf{1}}U_\infty t)], \tag{3.1}$$

where

$$\hat{\mathbf{u}}^\infty = \{\hat{u}_1^\infty, \hat{u}_2^\infty, \hat{u}_3^\infty\}$$

is a constant such that† can always be written as

$$\hat{\mathbf{u}}^\infty.\mathbf{k} = 0,$$

$$u_i = \mathscr{M}_{ij}(\mathbf{x}\,|\,\mathbf{k})\,\hat{u}_j^\infty\, e^{-ik_1 U_\infty t}; \tag{3.2}$$

here and in all subsequent formulae, repeated indices indicate summations from 1 to 3. The tensor $\mathscr{M}_{ij}$ acts like a transfer function that relates the local and upstream velocity fields.

It has been shown by Batchelor & Proudman (1954) and by Hunt (1973) that a homogeneous but otherwise arbitrary random velocity fluctuation imposed on the upstream flow will produce a downstream turbulent flow whose velocity correlation

$$R_{ij}(\mathbf{x},\mathbf{x}',\tau) \equiv \overline{u_i(\mathbf{x},t)\,u_j(\mathbf{x}',t+\tau)} \tag{3.3}$$

† This condition follows from the requirement that $\mathbf{u}_\infty$ be solenoidal.

is related to the spectrum

$$\Phi_{ij}^{(\infty)}(\mathbf{k}) \equiv \frac{1}{(2\pi)^3}\iiint_{-\infty}^{\infty} R_{ij}^{(\infty)}(\mathbf{y})\, e^{-i\mathbf{k}\cdot\mathbf{y}}\, d\mathbf{y} \tag{3.4}$$

of the upstream velocity covariance tensor

$$R_{ij}^{(\infty)}(\mathbf{y}) = \overline{u_{\infty i}(\mathbf{x}-\hat{\mathbf{1}}U_\infty t)\, u_{\infty j}(\mathbf{x}+\mathbf{y}-\hat{\mathbf{1}}U_\infty t)} \tag{3.5}$$

(which, owing to the assumed homogeneity, depends only on the indicated argument) by

$$R_{ij}(\mathbf{x},\mathbf{x}',\tau) \equiv \iiint_{-\infty}^{\infty} \mathscr{M}_{ik}^{*}(\mathbf{x}\mid\mathbf{k})\,\mathscr{M}_{jl}(\mathbf{x}'\mid\mathbf{k})\,\Phi_{kl}^{(\infty)}(\mathbf{k})\, e^{-ik_1 U_\infty \tau}\, d\mathbf{k}. \tag{3.6}$$

The asterisk denotes the complex conjugate. The one-dimensional spectrum

$$\Theta_{ij}(\mathbf{x},\mathbf{x}'\mid k_1) \equiv \frac{U_\infty}{2\pi}\int_{-\infty}^{\infty} R_{ij}(\mathbf{x},\mathbf{x}',\tau)\, e^{ik_1 U_\infty \tau}\, d\tau \tag{3.7}$$

is given by

$$\Theta_{ij}(\mathbf{x},\mathbf{x}'\mid k_1) = \iint_{-\infty}^{\infty} \mathscr{M}_{ik}^{*}(\mathbf{x}\mid\mathbf{k})\,\mathscr{M}_{jl}(\mathbf{x}'\mid\mathbf{k})\,\Phi_{kl}^{(\infty)}(\mathbf{k})\, dk_2\, dk_3. \tag{3.8}$$

4. Solutions for individual wavenumber components

Before calculating the turbulence spectra it is necessary to find the solution to the linearized equations (2.3), (2.7) and (2.8) for an upstream vortical velocity field of the type (3.1). We shall suppose that the mean potential flow is two-dimensional and incompressible, so that its velocity field **U** is given by

$$U_1 = \partial\Psi/\partial x_2, \quad U_2 = -\partial\Psi/\partial x_1, \quad U_3 = 0, \tag{4.1}$$

where the mean-flow stream function Ψ satisfies the two-dimensional Laplace's equation

$$\partial^2\Psi/\partial x_1^2 + \partial^2\Psi/\partial x_2^2 = 0. \tag{4.2}$$

Our interest here is in internal flows, such as those depicted in figure 2, that undergo significant contractions and have constant mutually parallel velocity fields far upstream and far downstream – say U_∞ and U_+, respectively. Then

$$\Psi \to U_\infty x_2 \quad \text{as} \quad x_1 \to -\infty \tag{4.3}$$

and

$$\Psi \to U_+ x_2 + \text{const.} = U_\infty x_2 c + \text{const.} \quad \text{as} \quad x_1 \to +\infty, \tag{4.4}$$

where

$$c = U_+/U_\infty = a/\delta \tag{4.5}$$

is the contraction ratio and a and δ are the transverse dimensions of the upstream and downstream flow passages (see figure 2). On the other hand, it follows from (2.6) that

$$X_1 \to x_1 \quad \text{as} \quad x_1 \to -\infty, \tag{4.6}$$

and

$$X_1 \to a\Delta_+(x_2/\delta) + x_1/c \quad \text{as} \quad x_1 \to +\infty, \tag{4.7}$$

where

$$\begin{aligned}\Delta_+(x_2/\delta) &\equiv \frac{U_\infty}{a}\left[\int_{-\infty}^{0}\left(\frac{1}{U_1}-\frac{1}{U_\infty}\right)dx_1 + \int_0^{\infty}\left(\frac{1}{U_1}-\frac{1}{U_+}\right)dx_1\right] \\ &= \int_{-\infty}^{0}\left(\frac{U_\infty}{U_1}-1\right)d\left(\frac{x_1}{a}\right) + \int_0^{\infty}\left(\frac{U_+}{U_1}-1\right)d\left(\frac{x_1}{\delta}\right),\end{aligned} \tag{4.8}$$

and the integration is carried out along the streamline that approaches the line x_2 = constant far downstream in the flow.

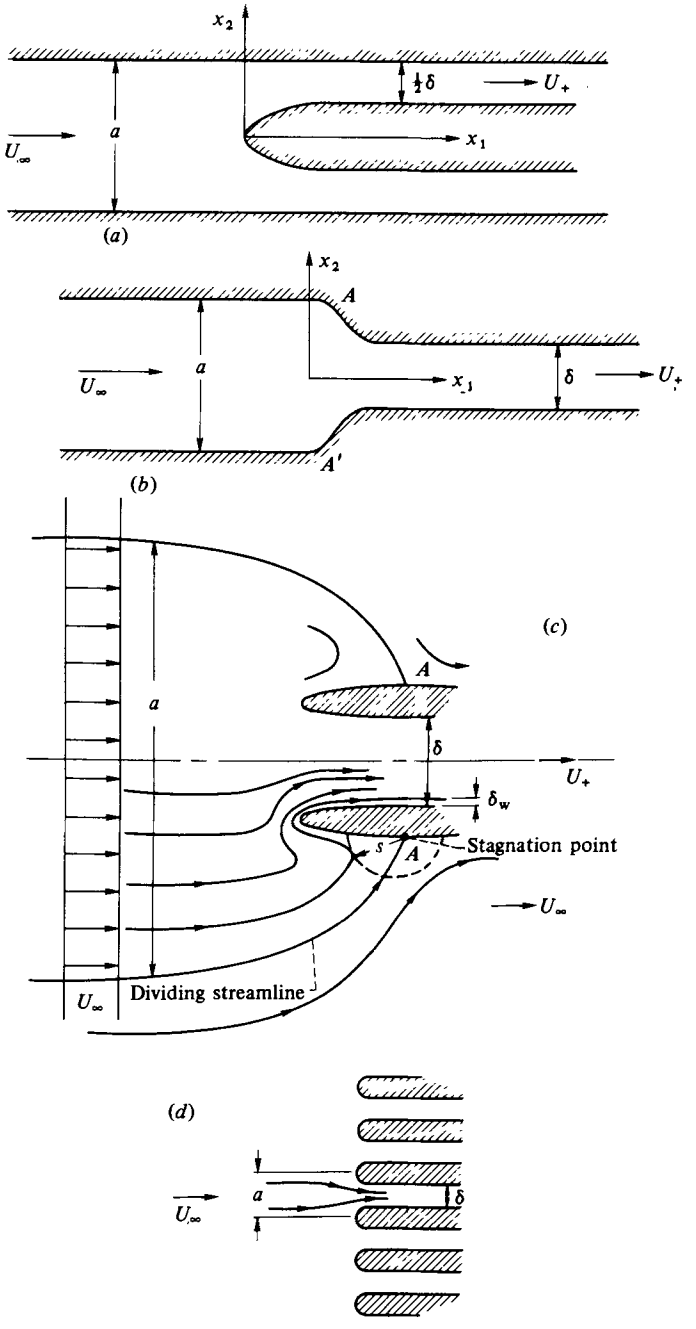

FIGURE 2. Some typical contracting streams. (*a*) Internal flow with branching contraction. (*b*) Internal flow with single continuous contraction. (*c*) Inlet flow. (*d*) Flow into a honeycomb-type structure.

Since the mean flow is two-dimensional we can set $X_2 = \Psi/U_\infty$ and $X_3 = x_3$. Then at downstream infinity the vortical velocity field (2.3) produced by the upstream harmonic vortical velocity field (3.1) becomes (to within an unimportant constant-phase factor)

$$\mathbf{u}^{(I)} \to \left\{\frac{\hat{u}_1^\infty}{c},\ c\hat{u}_2^\infty + a\hat{u}_1^\infty \Delta_+',\ \hat{u}_3^\infty\right\} e^{i[\mathbf{x}\cdot\mathbf{x}+k_1 a\Delta_+(x_2/\delta)-k_1 U_\infty t]} \quad \text{as} \quad \chi_1 \to \infty, \tag{4.9}$$

where

$$\boldsymbol{\chi} = \{\chi_1, \chi_2, \chi_3\} \equiv \{k_1/c, ck_2, k_3\}, \tag{4.10}$$

and the prime denotes differentiation with respect to x_2. In the downstream region the boundary condition (2.8) becomes (see figure 2)

$$\partial\phi/\partial x_2 = -u_2^{(I)} \quad \text{as} \quad x_2 \to \pm\tfrac{1}{2}\delta. \tag{4.11}$$

Then (4.9) and (4.11) imply that, as $x_1 \to \infty$, (2.7) will possess a solution of the form

$$\phi = \phi_0(x_2)\, e^{i(\chi_1 x_1 + \chi_3 x_3 - k_1 U_\infty t)}, \tag{4.12}$$

where ϕ_0 satisfies the ordinary differential equation

$$\phi_0'' - \gamma^2\phi_0 = -i\left(\frac{\hat{u}_1^\infty}{c}\chi_1 + \hat{u}_3^\infty \chi_3\right) e^{i(\chi_2 x_2 + k_1 a\Delta_+)} - [(c\hat{u}_2^\infty + a\hat{u}_1^\infty \Delta_+')\, e^{i(\chi_2 x_2 + k_1 a\Delta_+)}]', \tag{4.13}$$

subject to the boundary condition

$$\phi_0' \to -(c\hat{u}_2^\infty + a\hat{u}_1^\infty \Delta_+')\, e^{i(\chi_2 x_2 + k_1 a\Delta_+)} \quad \text{as} \quad x_2 \to \pm\tfrac{1}{2}\delta, \tag{4.14}$$

where

$$\gamma \equiv (\chi_3^2 + \chi_1^2)^{\frac{1}{2}}. \tag{4.15}$$

Equation (4.13) can be solved by standard methods to obtain

$$\phi_0 = \delta \int_{-\frac{1}{2}}^{\frac{1}{2}} \left[i\left(\frac{\hat{u}_1^\infty}{c}\chi_1 + \hat{u}_3^\infty \chi_3\right) \delta \mathscr{K}_1^+(y \mid \eta) + c\left(\hat{u}_2^\infty + \hat{u}_1^\infty \frac{d}{d\eta}\Delta_+(\eta)\right) \mathscr{K}_2^+(y \mid \eta)\right] e^{i\delta[\chi_2\eta + k_1 c\Delta_+(\eta)]}\, d\eta, \tag{4.16}$$

where

$$y \equiv x_2/\delta, \tag{4.17}$$

$$\mathscr{K}_1^\pm(y \mid \eta) \equiv \frac{\pm\cosh\gamma\delta(y+\eta) + \cosh\gamma\delta(1-|y-\eta|)}{2\gamma\delta\sinh\gamma\delta}, \tag{4.18}$$

$$\mathscr{K}_2^\pm(y \mid \eta) \equiv -\frac{\pm\sinh\gamma\delta(y+\eta) + \operatorname{sgn}(y-\eta)\sinh\gamma\delta(1-|y-\eta|)}{2\sinh\gamma\delta}. \tag{4.19}$$

It now follows from (2.1), (4.9), (4.10), (4.15) and (4.16) that the transfer coefficients defined by (3.2) are given by

$$\mathscr{M}_{ij}(\mathbf{x} \mid \mathbf{k}) = M_{ij}(y \mid \boldsymbol{\kappa}, c\boldsymbol{\kappa})\, e^{i(\chi_1 x_1 + \chi_3 x_3)}, \tag{4.20}$$

where

$$\left.\begin{aligned} &M_{11} = (\kappa_3^2 F_1^+ - ic\kappa_2 F_2^+)/c, \quad M_{12} = i\kappa_1 F_2^+, \quad M_{13} = -\kappa_1\kappa_3 F_1^+/c,\\ &M_{21} = -(i\kappa_3^2 F_2^- + c\kappa_2\tilde{\gamma}^2 F_1^-)/\kappa_1, \quad M_{22} = c\tilde{\gamma}^2 F_1^-, \quad M_{23} = i\kappa_3 F_2^-,\\ &M_{31} = \kappa_3[\kappa_3^2 F_1^+ - ic\kappa_2 F_2^+ - e^{ic(\kappa_2 y + \kappa_1\Delta_+(y))}]/\kappa_1, \quad M_{32} = ic\kappa_3 F_2^+,\\ &M_{33} = e^{ic(\kappa_2 y + \kappa_1\Delta_+(y))} - \kappa_3^2 F_1^+, \end{aligned}\right\} \tag{4.21}$$

$$\kappa_j \equiv \delta k_j \quad \text{for} \quad j = 1, 2, 3; \quad \tilde{\gamma} = (\kappa_3^2 + (\kappa_1/c)^2)^{\frac{1}{2}} \tag{4.22}$$

and
$$F_i^{\pm} \equiv \int_{-\frac{1}{2}}^{\frac{1}{2}} \mathscr{K}_i^{\pm}(y \mid \eta)\, e^{ic(\kappa_2\eta + \kappa_1 \Delta_+(\eta))}\, d\eta. \tag{4.23}$$

The three-dimensional spectrum $\Phi_{kl}^{(\infty)}$, which appears in (3.6), can be expressed as a function of $\mathbf{k}l_\infty$ and l_∞, where as we have indicated l_∞ denotes a characteristic spatial scale (say the integral scale) of the upstream turbulence. Upon putting $\mathbf{x}' = \mathbf{x}$ and $\tau = 0$ to obtain one-point covariances and using (4.17), (4.20) and (4.22), (3.6) becomes

$$R_{ij} = \frac{1}{\delta^3} \iiint_{-\infty}^{\infty} M_{ik}^*(y \mid \boldsymbol{\kappa}, c\boldsymbol{\kappa})\, M_{jl}(y \mid \boldsymbol{\kappa}, c\boldsymbol{\kappa})\, \Phi_{kl}^{(\infty)}(\sigma\boldsymbol{\kappa}, l_\infty)\, d\boldsymbol{\kappa}. \tag{4.24}$$

Here we have put $\sigma \equiv l_\infty/\delta$. Now (4.24) will generally lead to formulae that are too complex to be evaluated with a reasonable amount of computation. In the next two sections we therefore simplify results by considering the two asymptotic limits

$$\text{(i)} \quad c \to \infty, \quad \sigma = O(1), \quad y = O(1) \tag{4.25}$$

and
$$\text{(ii)} \quad \sigma^{-1} \to \infty, \quad c = O(1), \quad y = O(1). \tag{4.26}$$

In both these cases $\sigma/c = l_\infty/\delta \to 0$. The first corresponds to the case where the contraction is large and the turbulence length scale is finite and the second corresponds to the case where the turbulence spatial scale is small relative to both the upstream and downstream dimensions of the contraction but the contraction ratio is arbitrary.

Results given by Durbin (1979) can be used to prove that, as long as the integrals remain convergent,

$$\lim_{\substack{c\to\infty \\ \sigma = O(1)}} R_{ij} = \frac{1}{\delta^3} \iiint_{-\infty}^{\infty} \tilde{M}_{ik}^* \tilde{M}_{jl}\, \Phi_{kl}^{(\infty)}(\sigma\boldsymbol{\kappa}, l_\infty)\, d\boldsymbol{\kappa}, \tag{4.27a}$$

$$\lim_{\substack{\sigma\to 0 \\ c = O(1)}} R_{ij} = \frac{1}{\delta^3} \iiint_{-\infty}^{\infty} \tilde{\tilde{M}}_{ik}^* \tilde{\tilde{M}}_{jl}\, \Phi_{kl}^{(\infty)}(\sigma\boldsymbol{\kappa}, l_\infty)\, d\boldsymbol{\kappa}, \tag{4.27b}$$

where
$$\tilde{M}_{ij} \equiv \lim_{\substack{c\kappa_l \to \infty \\ |\boldsymbol{\kappa}| = O(1)}} M_{ij}(y \mid \boldsymbol{\kappa}, c\boldsymbol{\kappa}), \tag{4.28a}$$

and
$$\tilde{\tilde{M}}_{ij} \equiv \lim_{\substack{\kappa_l \to \infty \\ c\kappa_l \to \infty}} M_{ij}(y \mid \boldsymbol{\kappa}, c\boldsymbol{\kappa}). \tag{4.28b}$$

In appendix C we show that the limit of (4.27*a*) as $\sigma \to 0$ is essentially equal to the limit of (4.27*b*) as $c \to \infty$ even though

$$\lim_{\kappa_l \to \infty} \tilde{M}_{ij} \neq \lim_{c\to\infty} \tilde{\tilde{M}}_{ij}.$$

5. Large contraction-ratio limit

Batchelor & Proudman (1954) considered the case of homogeneously distorted turbulence. They showed that in this limit the asymptotic formulae for a large contraction ratio provide a good approximation to the formulae for an arbitrary contraction ratio over the range $c > 2$. It is therefore reasonable to simplify the formula (4.24) for the case where l_∞/δ is finite by taking the large contraction-ratio limit (4.27*a*).

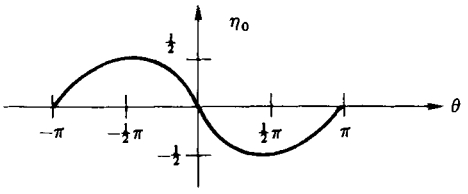

FIGURE 3. Variation of η_0 with θ for the case where A and A' are stagnation points in figure 2.

Now, it can be seen from (4.8) that $\Delta_+(\eta)$ is of order one as $c \to \infty$ for $-\frac{1}{2} < \eta < \frac{1}{2}$ (see also specific examples worked out in appendices A and B). Hence, letting

$$\kappa_0 \equiv (\kappa_1^2 + \kappa_2^2)^{\frac{1}{2}}, \tag{5.1}$$

introducing the polar angle θ by

$$\kappa_1 = \kappa_0 \cos\theta, \quad \kappa_2 = \kappa_0 \sin\theta, \tag{5.2), (5.3}$$

and using the method of stationary phase (Erdélyi 1956) to evaluate (4.23) for large $\kappa_0 c$, we obtain

$$F_i^{\pm} \sim \left[\frac{2\pi}{\Delta_+''(\eta_0)\, c\kappa_1}\right]^{\frac{1}{2}} \mathscr{K}_i^{\pm}(y \mid \eta_0)\, e^{ic[\eta_0\kappa_1 + \Delta_+(\eta_0)\kappa_2]} \quad \text{as} \quad \kappa_0 c \to \infty, \tag{5.4}$$

where η_0 is a solution of

$$\Delta_+'(\eta_0) = -\tan\theta \tag{5.5}$$

and the primes now denote differentiation with respect to η_0.

For flow into an inlet or for internal flows with stagnation points (at the points A and A' in figure 2*b*), $\Delta_+'(\eta)$ will go to infinity at the end points $\eta = \pm\frac{1}{2}$ and θ will therefore equal $\mp\frac{1}{2}\pi$ when $\eta_0 = \pm\frac{1}{2}$. Then, the variation of η_0 with θ will be as shown in figure 3. The examples worked out in appendices A and B correspond to this case.

The transfer coefficients (4.21) now become

$$\left.\begin{aligned} M_{11} &= -i\kappa_2 F_2^+ + O((\kappa_0 c)^{-\frac{3}{2}}), \quad M_{12} = i\kappa_1 F_2^+, \quad M_{13} = O((\kappa_0 c)^{-\frac{3}{2}}), \\ M_{21} &= -c\kappa_2 \kappa_1^{-1} \tilde{\gamma}^2 F_1^- + O((\kappa_0 c)^{-\frac{1}{2}}), \quad M_{22} = c\tilde{\gamma}^2 F_1^-, \quad M_{23} = O((\kappa_0 c)^{-\frac{1}{2}}), \\ M_{31} &= -ic\frac{\kappa_2\kappa_3}{\kappa_1} F_2^+ + O(1), \quad M_{32} = ic\kappa_3 F_2^+, \quad M_{33} = O(1). \end{aligned}\right\} \tag{5.6}$$

Inserting (5.4) and (5.6) into (4.24) and using (3.3) we find that

$$\left.\begin{aligned} \overline{u_1^2}(\mathbf{x}, t) = R_{11}(\mathbf{x}, \mathbf{x}, 0) &= \frac{1}{2c} \iiint_{-\infty}^{\infty} \frac{H(\boldsymbol{\kappa})}{\Delta_+''(\eta_0)\,\kappa_1} [\mathscr{K}_2^+(y \mid \eta_0)]^2 \, d\boldsymbol{\kappa}, \\ \overline{u_2^2} &= \frac{c}{2} \iiint_{-\infty}^{\infty} \frac{H(\boldsymbol{\kappa})}{\Delta_+''(\eta_0)\,\kappa_1} [\tilde{\gamma}\mathscr{K}_1^-(y \mid \eta_0)]^2 \left(\frac{\tilde{\gamma}}{\kappa_1}\right)^2 d\boldsymbol{\kappa}, \\ \overline{u_3^2} &= \frac{c}{2} \iiint_{-\infty}^{\infty} \frac{H(\boldsymbol{\kappa})}{\Delta_+''(\eta_0)\,\kappa_1} [\mathscr{K}_2^+(y \mid \eta_0)]^2 \left(\frac{\kappa_3}{\kappa_1}\right)^2 d\boldsymbol{\kappa}, \end{aligned}\right\} \tag{5.7}$$

where we have put

$$H(\boldsymbol{\kappa}) \equiv \frac{4\pi}{\delta^3}(\kappa_2^2 \Phi_{11}^{(\infty)} - 2\kappa_1\kappa_2 \Phi_{12}^{(\infty)} + \kappa_1^2 \Phi_{22}^{(\infty)}). \tag{5.8}$$

Similarly, inserting (5.4) and (5.6) into (3.8), we obtain

$$\left.\begin{aligned}\Theta_{11} &= \frac{\delta}{2c}\iint_{-\infty}^{\infty}\frac{H(\boldsymbol{\kappa})}{\Delta_+''(\eta_0)\,\kappa_1}\,[\mathscr{K}_2^+(y\mid\eta_0)]^2\,d\kappa_2\,d\kappa_3,\\ \Theta_{22} &= \frac{c\delta}{2}\iint_{-\infty}^{\infty}\frac{H(\boldsymbol{\kappa})}{\Delta_+''(\eta_0)\,\kappa_1}\,[\tilde{\gamma}\mathscr{K}_1^-(y\mid\eta_0)]^2\left(\frac{\tilde{\gamma}}{\kappa_1}\right)^2 d\kappa_2\,d\kappa_3,\\ \Theta_{33} &= \frac{c\delta}{2}\iint_{-\infty}^{\infty}\frac{H(\boldsymbol{\kappa})}{\Delta_+''(\eta_0)\,\kappa_1}\,[\mathscr{K}_2^+(y\mid\eta_0)]^2\left(\frac{\kappa_3}{\kappa_1}\right)^2 d\kappa_2\,d\kappa_3.\end{aligned}\right\}\tag{5.9}$$

We shall now restrict our attention to the case depicted in figure 3 where $\eta_0 \to \pm\frac{1}{2}$ when $\theta \to \mp\frac{1}{2}\pi$. Since

$$d\boldsymbol{\kappa} = d\kappa_3\kappa_0\,d\kappa_0\,d\theta$$

while it follows from (5.5) that

$$d\theta/\cos^2\theta = -\Delta_+''(\eta_0)\,d\eta_0$$

and that

$$\cos\theta = \pm[1+[\Delta_+'(\eta_0)]^2]^{-\frac{1}{2}},$$

we can change variables of integration in (5.7) to obtain

$$\left.\begin{aligned}\overline{u_1^2} &= \frac{1}{c}\int_{-\infty}^{\infty}\int_{-\frac{1}{2}}^{\frac{1}{2}}\int_0^{\infty}\frac{H(\boldsymbol{\kappa})}{(1+[\Delta_+'(\eta_0)]^2)^{\frac{1}{2}}}\,[\mathscr{K}_2^+(y\mid\eta_0)]^2\,d\kappa_0\,d\eta_0\,d\kappa_3,\\ \overline{u_2^2} &= c\int_{-\infty}^{\infty}\int_{-\frac{1}{2}}^{\frac{1}{2}}\int_0^{\infty}\frac{H(\boldsymbol{\kappa})\,(1+[\Delta_+'(\eta_0)]^2)^{\frac{1}{2}}}{\kappa_0^2}\,[\tilde{\gamma}^2\mathscr{K}_1^-(y\mid\eta_0)]^2\,d\kappa_0\,d\eta_0\,d\kappa_3,\\ \overline{u_3^2} &= c\int_{-\infty}^{\infty}\int_{-\frac{1}{2}}^{\frac{1}{2}}\int_0^{\infty}\frac{H(\boldsymbol{\kappa})\,(1+[\Delta_+'(\eta_0)]^2)^{\frac{1}{2}}}{\kappa_0^2}\,[\kappa_3\mathscr{K}_2^+(y\mid\eta_0)]^2\,d\kappa_0\,d\eta_0\,d\kappa_3.\end{aligned}\right\}\tag{5.10}$$

Similarly, since it follows from (5.3) and (5.5) that

$$d\kappa_2 = \kappa_1\Delta_+''(\eta_0)\,d\eta_0,$$

we can change variables of integration in (5.9) to obtain

$$\left.\begin{aligned}\Theta_{11} &= \frac{\delta}{2c}\int_{-\infty}^{\infty}\int_{-\frac{1}{2}}^{\frac{1}{2}}H(\boldsymbol{\kappa})\,[\mathscr{K}_2^+(y\mid\eta_0)]^2\,d\eta_0\,d\kappa_3,\\ \Theta_{22} &= \frac{c\delta}{2}\int_{-\infty}^{\infty}\int_{-\frac{1}{2}}^{\frac{1}{2}}H(\boldsymbol{\kappa})\left[\frac{\tilde{\gamma}^2}{\kappa_1}\mathscr{K}_1^-(y\mid\eta_0)\right]^2 d\eta_0\,d\kappa_3,\\ \Theta_{33} &= \frac{c\delta}{2}\int_{-\infty}^{\infty}\int_{-\frac{1}{2}}^{\frac{1}{2}}H(\boldsymbol{\kappa})\left[\frac{\kappa_3}{\kappa_1}\mathscr{K}_2^+(y\mid\eta_0)\right]^2 d\eta_0\,d\kappa_3.\end{aligned}\right\}\tag{5.11}$$

When the upstream turbulence is isotropic

$$\Phi_{ij}^{(\infty)} = \frac{E(k)}{4\pi k^4}(\delta_{ij}k^2 - k_ik_j).$$

Substitution of this into (5.8) gives

$$H(\boldsymbol{\kappa}) = \frac{E(k)}{\delta^3k^2}\kappa_0^2.\tag{5.12}$$

Now, except as explained in appendix C, we can replace $\tilde{\gamma} \equiv (\kappa_3^2+(\kappa_1/c)^2)^{\frac{1}{2}}$ by $|\kappa_3|$ for large values of c. Then, $\mathscr{K}_j^{\pm}$ for $j = 1, 2$ will be independent of κ_0 and, when the up-

stream turbulence is isotropic, we can use the fact that $E(k)/k^2$ depends only on $k^2 = (\kappa_0^2+\kappa_3^2)/\delta^2$ to write (5.10) in the form

$$\overline{u_1^2} = \frac{1}{c}\int_{-\infty}^{\infty}\int_{-\frac{1}{2}}^{\frac{1}{2}} \frac{[\mathscr{K}_2^+(y\mid\eta_0)]^2}{(1+[\Delta_+'(\eta_0)]^2)^{\frac{1}{2}}} I(\kappa_3)\,d\eta_0\,d\kappa_3, \tag{5.13a}$$

$$\overline{u_2^2} = -c\int_{-\infty}^{\infty}\int_{-\frac{1}{2}}^{\frac{1}{2}} (1+[\Delta_+'(\eta_0)]^2)^{\frac{1}{2}}[\kappa_3^2\mathscr{K}_1^-(y\mid\eta_0)]^2\frac{1}{\kappa_3}\frac{dI(\kappa_3)}{d\kappa_3}\,d\eta_0\,d\kappa_3, \tag{5.13b}$$

$$\overline{u_3^2} = -c\int_{-\infty}^{\infty}\int_{-\frac{1}{2}}^{\frac{1}{2}} (1+[\Delta_+'(\eta_0)]^2)^{\frac{1}{2}}[\kappa_3\mathscr{K}_2^+(y\mid\eta_0)]^2\frac{1}{\kappa_3}\frac{d}{d\kappa_3}I(\kappa_3)\,d\eta_0\,d\kappa_3, \tag{5.13c}$$

where
$$I(\kappa_3) = \frac{1}{\delta^3}\int_0^{\infty}\kappa_0^2\frac{E(k)}{k^2}\,d\kappa_0. \tag{5.14}$$

For the Kolmogorov spectrum

$$E(k) = \frac{55}{9\pi}\frac{\overline{u_{\infty 1}^2}\,g_2(g_2/l_\infty)^{\frac{2}{3}}k^4}{[(g_2/l_\infty)^2+k^2]^{\frac{17}{6}}}, \tag{5.15}$$

where $g_2 = \pi^{\frac{1}{2}}\Gamma(\frac{5}{6})/\Gamma(\frac{1}{3})$ and l_∞ is the integral scale,

$$I(\kappa_3) = \overline{u_{\infty 1}^2}\frac{\alpha^{\frac{2}{3}}}{3}\frac{\kappa_3^2+\frac{9}{2}(\kappa_3^2+\alpha^2)}{(\kappa_3^2+\alpha^2)^{\frac{4}{3}}}, \tag{5.16}$$

where
$$\alpha \equiv g_2(\delta/l_\infty).$$

6. Small-scale turbulence: quasi-homogeneous limit

We now consider the case (4.27*b*) where $\kappa \gg 1$ and $c = O(1)$. This is analogous to the classical theory of homogeneously distorted turbulence that was developed by Ribner & Tucker (1953) and Batchelor & Proudman (1954).

When $\tilde{\gamma}$ is large

$$\mathscr{K}_1^{\pm} \to \frac{e^{-\tilde{\gamma}|y-\eta|}}{2\tilde{\gamma}}; \quad \mathscr{K}_2^{\pm} \to -\operatorname{sgn}(y-\eta)\frac{e^{-\tilde{\gamma}|y-\eta|}}{2}. \tag{6.1}$$

Then the principal contribution to the integral in (4.23) comes from the vicinity of $\eta = y$ and we can therefore replace $\Delta_+(\eta)$ by $\Delta_+(y)+\Delta_+'(y)(\eta-y)$ to obtain

$$F_1^{\pm} \sim \frac{e^{ic[(\kappa_2 y+\kappa_1\Delta_+(y)]}}{\tilde{\chi}^2}; \quad F_2^{\pm} \sim -\frac{e^{ic[\kappa_2 y+\kappa_1\Delta_+(y)]}}{i\tilde{\chi}^2}\tilde{\chi}_2, \tag{6.2}$$

where $\tilde{\chi}_2 = c[\kappa_2+\kappa_1\Delta_+'(y)]$ and $\tilde{\chi}^2 = \tilde{\gamma}^2+\tilde{\chi}_2^2$. Then

$$M_{ij} = \frac{\tilde{\chi}_m\tilde{\chi}_n}{\tilde{\chi}^2}\epsilon_{kni}\epsilon_{kml}T_{lj}e^{ic[\kappa_2 y+\kappa_1\Delta_+]}, \tag{6.3}$$

where ϵ_{ijk} is the permutation tensor,

$$T_{lj} = \begin{bmatrix} \frac{1}{c} & 0 & 0 \\ c\Delta_+'(y) & c & 0 \\ 0 & 0 & 1 \end{bmatrix}, \tag{6.4}$$

and (see (4.10))
$$\tilde{\chi}_1 = \chi_1 = \kappa_1/c, \quad \tilde{\chi}_3 = \kappa_3 = \chi_3,$$

so that
$$\tilde{\chi}_i = T_{ij}\kappa_j.$$

It is shown in appendix D that (6.3) can be transformed into the formula used by Hunt† (1973) and by Batchelor & Proudman (1954). It could have been obtained more directly as the high-frequency solution of (2.7) with (2.3)–(2.5) and (3.1) inserted (see, for example, Goldstein 1979).

Using (6.3) in (3.3) and (4.24), assuming that the upstream turbulence is isotropic, introducing polar co-ordinates and carrying out the integration with respect to the radial co-ordinate, we obtain see (4.10))

$$\left.\begin{aligned}
\frac{\overline{u_1^2}}{u_{\infty 1}^2} &= \frac{3}{8\pi}\iint \frac{c^{-2}(\tilde{\chi}_3^2+\chi_2\tilde{\chi}_2)^2+\tilde{\chi}_1^2(\tilde{\chi}_3^2+c^2\tilde{\chi}_2^2)}{\tilde{\chi}^4}\,dS(\mathbf{k}),\\
\frac{\overline{u_2^2}}{u_{\infty 1}^2} &= \frac{3}{8\pi}\iint \frac{c^{-2}(c^2\Delta'_+\tilde{\chi}_3^2-\chi_2\tilde{\chi}_1)^2+c^2(\tilde{\chi}_3^2+\tilde{\chi}_1^2)^2+\tilde{\chi}_3^2\tilde{\chi}_2^2}{\tilde{\chi}^4}\,dS(\mathbf{k}),\\
\frac{\overline{u_3^2}}{u_{\infty 1}^2} &= \frac{3}{8\pi}\iint \frac{\tilde{\chi}_3^2[c^{-2}(c^2\Delta'_+\tilde{\chi}_2+\tilde{\chi}_1)^2+c^2\tilde{\chi}_2^2]+(\tilde{\chi}_1^2+\tilde{\chi}_2^2)^2}{\tilde{\chi}^4}\,dS(\mathbf{k}),
\end{aligned}\right\} \tag{6.5}$$

where the integration is carried out over the unit sphere $k = 1$.

These results are essentially given by Batchelor & Proudman (1954). A similar formula can be written down for the turbulent shear stress $\overline{u_1u_2}/\overline{u_{\infty 1}^2}$. Upon introducing the polar co-ordinates

$$\left.\begin{aligned}
\kappa_1 &= \kappa\cos\phi\cos(\tilde{\theta}-\theta_0),\\
\kappa_2 &= \kappa\cos\phi\sin(\tilde{\theta}-\theta_0),\\
\kappa_3 &= \kappa\sin\phi,
\end{aligned}\right\} \tag{6.6}$$

where
$$\tan\theta_0 = D+(\operatorname{sgn}\Delta'_+)(D^2+1)^{\frac{1}{2}}, \tag{6.7}$$

and
$$D \equiv \left[\frac{1}{c^2}+c^2(\Delta_+'^2-1)\right]\Big/2c^2\Delta'_+, \tag{6.8}$$

we find that
$$\tilde{\chi}^2 = (\lambda_1/e_1)^2+(\lambda_2/e_2)^2+\lambda_3^2, \tag{6.9}$$

where
$$\lambda_1 = \kappa\cos\phi\cos\tilde{\theta},\quad \lambda_2 = \kappa\cos\phi\sin\tilde{\theta},\quad \lambda_3 = \kappa_3, \tag{6.10}$$

and
$$e_1 = \frac{1}{c(1-\Delta'_+(y)\cot\theta_0)^{\frac{1}{2}}},\quad e_2 = \frac{1}{c(1+\Delta'_+(y)\tan\theta_0)^{\frac{1}{2}}}. \tag{6.11}$$

Notice that
$$e_1e_2 = 1;\quad e_1 > e_2. \tag{6.12}$$

Inserting these results into (6.5) and the corresponding formula for the turbulent shear stress, we obtain

$$\left.\begin{aligned}
\frac{\overline{u_1^2}}{u_{\infty 1}^2} &= \cos^2\theta^\dagger\mu_1+\sin^2\theta^\dagger\mu_2,\\
\frac{\overline{u_2^2}}{u_{\infty 1}^2} &= \sin^2\theta^\dagger\mu_1+\cos^2\theta^\dagger\mu_2,\\
\frac{\overline{u_3^2}}{u_{\infty 1}^2} &= \mu_3,\\
\frac{\overline{u_1u_2}}{u_{\infty 1}^2} &= \cos\theta^\dagger\sin\theta^\dagger(\mu_2-\mu_1),
\end{aligned}\right\} \tag{6.13}$$

† Equation (D 1) is exactly the same as Hunt's equation (5.45*b*). This can be seen by noting that Hunt's γ_{mk} in his equation (3.11) is equal to the transpose of our T_{mk}^{-1}.

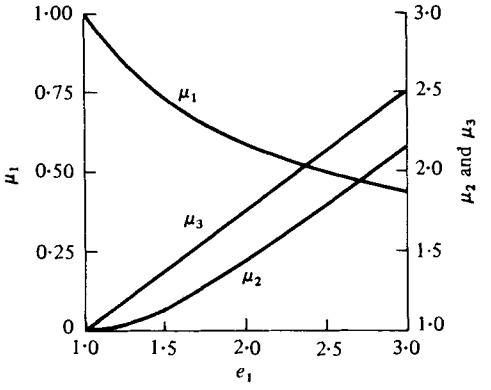

FIGURE 4. Intensity changes for bisymmetric two-dimensional contraction (from Batchelor & Proudman 1954).

where we have put

$$\cos\theta^\dagger = \frac{e_1}{c}\cos\theta_0 < 1, \tag{6.14}$$

$$\sin\theta^\dagger = \frac{e_2}{c}\sin\theta_0 = \left(1-\frac{e_1^2}{c^2}\cos^2\theta_0\right)^{\frac{1}{2}} \tag{6.15}$$

$$\mu_1 \equiv \frac{3}{8\pi}\iint \frac{e_1^{-2}(\lambda_3^2+\lambda_2^2/e_2^2)+(\lambda_1/e_1)^2(\lambda_3^2+\lambda_2^2/e_2^4)}{[(\lambda_1/e_1)^2+(\lambda_2/e_2)^2+\lambda_3^2]^2}\,dS(\boldsymbol{\lambda}),$$

$$\mu_2 = \frac{3}{8\pi}\iint \frac{e_1^{-2}(\lambda_1\lambda_2/e_1e_2)^2+e_2^{-2}(\lambda_3^2+\lambda_1^2/e_1^2)^2+\lambda_3^2(\lambda_2/e_2)^2}{[(\lambda_1/e_1)^2+(\lambda_2/e_2)^2+\lambda_3^2]^2}\,dS(\boldsymbol{\lambda}),$$

and

$$\mu_3 = \frac{3}{8\pi}\iint \frac{e_1^{-2}(\lambda_3\lambda_1/e_1)^2+(\lambda_3\lambda_2/e_2^2)^2+(\lambda_1/e_1)^2+(\lambda_2/e_2)^2}{[(\lambda_1/e_1)^2+(\lambda_2/e_2)^2+\lambda_3^2]^2}\,dS(\boldsymbol{\lambda}),$$

are the mean-square velocity ratios in the directions of principal strain that were evaluated by Batchelor & Proudman.† They are given in terms of elliptic integrals by their equations (5.13)–(5.15): their c corresponds to our e_1. For $e_1 > 2$ Batchelor & Proudman's large contraction-ratio asymptotic formulae (5.19) can be used with acceptable accuracy and for smaller values of e_1 the μ's can be obtained from their figure 3 which for convenience is reproduced here as figure 4.

The transformation described above was, in a sense, suggested by Batchelor & Proudman (1954); but their argument was not strictly correct since turbulence properties such as the one-dimensional spectra cannot be related to those of a symmetric contraction. (These quantities must be calculated directly by substituting (6.3) via (4.20) into (3.8).) In particular (6.13) shows that a general two-dimensional distortion can be decomposed into a plane strain, with strain-ratio $e_1(y)$, *followed by* a rotation through $-\theta^\dagger(y)$. (Actually, the straining is *preceded* by a rotation through $\theta_0(y)$; but the isotropic turbulence is invariant under this transformation.)

Suppose first that

$$c^\dagger \equiv c(1+\Delta_+'^2)^{\frac{1}{2}} \to \infty.$$

† Batchelor & Proudman (1954) actually derived these results for a constant area contraction, but they also apply to two-dimensional contraction when the x_3 direction is taken to be the cross-channel direction.

This will occur when $c \to \infty$ or when $\Delta'_+ \to \infty$. It follows from (6.8) and (6.11) that $e_1 \to c(\Delta'^2_+ + 1)^{\frac{1}{2}}$, $e_2 \to 1/e_1$, $\cos\theta_0 \to (1+\Delta'^2_+)^{-\frac{1}{2}}$ and $\sin\theta_0 \to \Delta'_+(1+\Delta'^2_+)^{-\frac{1}{2}}$. Hence, it follows from (6.14) and (6.15) that

$$\cos\theta^\dagger \to 1, \quad \sin\theta^\dagger \to 0 \quad \text{and} \quad \cos\theta^\dagger \sin\theta^\dagger \to \Delta'_+/c^2(1+\Delta'^2_+).$$

Using these in conjunction with Batchelor & Proudman's asymptotic formulae for μ_1, μ_2 and μ_3, we obtain

$$\left.\begin{aligned} &\frac{\overline{u_1^2}}{u_{\infty 1}^2} \to \frac{3}{4c^\dagger}(\ln 4c^\dagger - 1) \\ &\frac{\overline{u_2^2}}{u_{\infty 1}^2}, \frac{\overline{u_3^2}}{u_{\infty 1}^2} \to \tfrac{3}{4}c^\dagger \\ &\frac{\overline{u_1 u_2}}{u_{\infty 1}^2} \to \frac{3}{4}\frac{\Delta'_+}{c^\dagger} \end{aligned}\right\} \quad \text{as} \quad c^\dagger \to \infty. \tag{6.16}$$

As we have already indicated the one-dimensional spectra must be calculated directly from (3.8). Thus, substituting (6.3) in (4.20); using the result in (3.8); taking the limit $c \to \infty$; and using the complementary Watson's lemma developed by Durbin (1979), we obtain, after considerable manipulation,

$$\begin{aligned} \Theta_{11} \to{}& \frac{\pi k_1^2 g_3[1+\Delta'^2_+]u_{\infty 1}^2 l_\infty}{c[g_2+k_1^2(1+\Delta'^2_+)]^{\frac{11}{6}}}\left\{\frac{3}{11} - \frac{k_1(1+\Delta'^2_+)}{2(g_2+k_1^2(1+\Delta'^2_+))}\right. \\ &\times\left.\left[\psi(17/6)-\psi(1)-\ln\left(\frac{g_2+k_1^2(1+\Delta'^2_+)}{k_1^2(1+\Delta'^2_+)}\right)\right]-\ln(4c^2(1+\Delta'^2_+))\right\} \\ &+\left\{\begin{array}{ll} \dfrac{1}{2c^2}\displaystyle\sum_1^3 \Theta_{ii}^{(\infty)}(k_1) & \text{for} \quad k_1 c = O(1) \\ 0 & \text{for} \quad k_1 = O(1) \end{array}\right\} \quad \text{as} \quad c \to \infty, \end{aligned} \tag{6.17a}$$

$$\Theta_{33} \to \Theta_{22} \to \frac{c}{4}(1+\Delta'^2_+)\sum_{i=1}^{3}\Theta_{ii}^{(\infty)}(k_1[1+\Delta'^2_+]^{\frac{1}{2}}) \quad \text{as} \quad c \to \infty, \tag{6.17b}$$

where $\psi(X)$ denotes the logarithmic derivative of the gamma function,

$$g_3 = 55g_2^{\frac{5}{3}}/36\pi^2$$

and k_1 is non-dimensionalized by l_∞. When $k_1 = O(1)$ the spectra (6.17*a*) and (6.17*b*) can be written in the form

$$\Theta_{ii} = (1+\Delta'^2_+)^{\frac{1}{2}}\,\text{function}\,(c^\dagger, k_1(1+\Delta'^2_+)^{\frac{1}{2}}).$$

This shows that, in addition to increasing the effective strain from c to $c^\dagger$, the drift function gradient acts to compress the turbulent energy into the low-frequency portion of the spectrum where $k_1(1+\Delta'^2_+)^{\frac{1}{2}} = O(1)$. The $O(c^{-2})$ term in (6.17*a*) for $k_1 c = O(1)$ has been retained because the remaining terms go to zero like k_1^2 as $k_1 \to 0$. In fact, it is easy to show (by substituting (6.3) via (4.20) into (3.8)) that even when c is arbitrary

$$\frac{\Theta_{11}(0)}{\Theta_{11}^\infty(0)} = 1/c^2, \tag{6.17c}$$†

$$\frac{\Theta_{22}(0)}{\Theta_{11}^\infty(0)} = \frac{c(1+\Delta'^2_+)}{2} - \frac{\Delta'^2_+ c}{2(c+1)^2}, \tag{6.17d}$$

$$\frac{\Theta_{33}(0)}{\Theta_{11}^\infty(0)} = \frac{c(1+\Delta'^2_+)}{2} - \frac{\Delta'^2_+(2c+1)c}{2(c+1)^2}. \tag{6.17e}$$

† (6.17*c*) is given incorrectly by Townsend (1976) as $1/c$.

Thus, it is not true in general that $\Theta_{22} = \Theta_{33}$. Curiously enough, the drift has no effect on the streamwise integral scale, $\Theta_{11}(0)$. As $c \to 1$ the drift increases $\Theta_{22}(0)$, more than $\Theta_{33}(0)$. As $c \to \infty$ the drift increases both $\Theta_{22}(0)$ and $\Theta_{33}(0)$ by the same amount.

Now, suppose that $c \to 1$ and that $\frac{1}{2} - |y| \gg c - 1$. Then it follows from (6.8) and (6.11) that $e_1 \to c$ and

$$\sin\theta_0 \to \frac{\Delta'_+}{\left[\Delta'^2_+ + 4\left(c - \frac{1}{c}\right)^2\right]^{\frac{1}{2}}},$$

$$\cos\theta_0 \to \frac{2(c - c^{-1})}{[\Delta'^2_+ + 4(c - c^{-1})^2]^{\frac{1}{2}}}.$$

But $\Delta_+ = O((c - c^{-1})^2)$ as $c \to 1$ so that $\cos\theta^\dagger = 1 + O((c - c^{-1})^2)$, $\sin\theta^\dagger \to 0$ and

$$\sin\theta^\dagger \cos\theta^\dagger \to \Delta'_+/2(c - c^{-1}).$$

Hence

$$\frac{\overline{u_1^2}}{u_{\infty 1}^2} \to \mu_i(c) \quad \text{for} \quad i = 1, 2, 3 \tag{6.18}$$

and

$$\frac{\overline{u_1 u_2}}{u_{\infty 1}^2} = \tfrac{2}{5}\Delta'_+. \tag{6.19}$$

The μ_i in (6.18) can be evaluated by using Townsend's (1976) formula (3.11.9) provided terms of $O((c - c^{-1})^2)$ are ignored. These expressions have been used to obtain (6.19).

In both of the limits $c^\dagger \to \infty$ and $c \to 1$, $\theta^\dagger \to 0$ and the principal directions of the correlation tensor $\overline{u_i u_j}$ coincide with the co-ordinate directions x_1, x_2, x_3 as they would for a symmetric contraction. On the other hand higher-order terms must be retained when evaluating the directional factor $\cos\theta^\dagger \sin\theta^\dagger$ for the turbulent shear stress. In this sense $\overline{u_1 u_2}$ is produced by effects of higher order than those producing the u_i^2.

7. Results and discussion

The results of the previous two sections were used to calculate the mean-square turbulence velocity ratios and turbulence spectra as functions of transverse distance across the downstream channel. The upstream turbulence was assumed to be isotropic, but this is not essential – any homogeneous turbulence distribution could have been considered.

7.1. *Large contraction-ratio limit*

Figures 5–7 are plots of the mean-square velocity ratios for the case where the contraction ratio is large but the turbulence spatial scale is arbitrary. The corresponding one-dimensional spectra at the centre-line of the channel and halfway across the channel are shown in figures 8–10. The drift function derivative Δ'_+ is calculated from the large-c asymptotic expansion (A 8). This result was derived for the channel flow shown in figure 15. But it is exactly the same as the large-c asymptotic expansion of Δ'_+ for the two-dimensional idealized inlet flow† analysed in appendix B and depicted in figure 16. It is easy to see that the channel-flow solution also represents the flow in the branching contraction shown in figure 2(*a*) and the flow into the infinite cascade

† The real flow into this type of inlet would, of course, tend to separate but we can interpret this flow as an idealized model of an actual unseparated inlet flow.

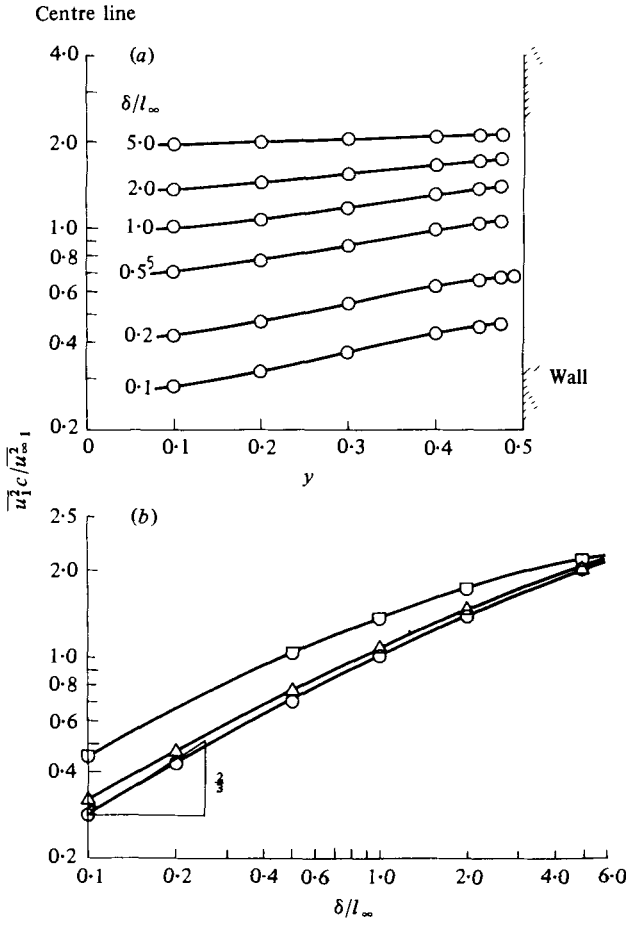

FIGURE 5. Mean-square streamwise turbulent velocity ratio for large contraction ratio and finite turbulence scale. (*b*) ○, $y = 0{\cdot}1$; △, $y = 0{\cdot}2$; ▽, $y = 0{\cdot}45$.

shown in figure 2(*d*). The latter configuration might represent a honeycomb-type turbulence control device. Figures 5–10, therefore, apply to both inlet flows and internal flows. Notice that there is a stagnation point upstream of the contraction in both the flows alluded to above. Viscous effects will set up a recirculation region which eliminates the stagnation point in the non-branching internal flow. But the present model should still serve as a good approximation to the real flow.

As can be seen from (5.11)–(5.15), the mean-square streamwise velocities along with their spectra are inversely proportional to c while the mean-square transverse velocities and spectra are directly proportional to c. The quantities plotted in figures 5–10 are therefore independent of contraction ratio.

The amplification of the transverse velocity components can be understood in terms of the vorticity amplification produced by the non-uniform mean flow. Thus, the surfaces of constant drift function, which coincide with the mean-flow fluid surfaces that were initially perpendicular to the flow when they were at upstream infinity, are bent over by the retardation of the mean flow at the upstream corner C shown in

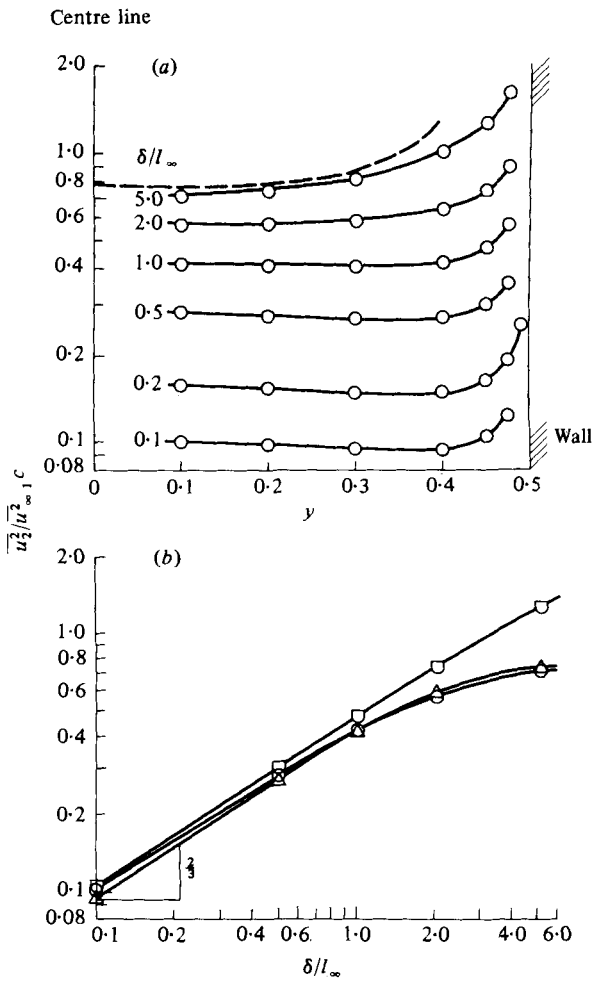

FIGURE 6. Mean-square transverse turbulence velocity ratio for large contraction ratio and arbitrary turbulent scale. (*b*) ○, $y = 0{\cdot}1$; △, $y = 0{\cdot}3$; ▽, $y = 0{\cdot}45$.

figure 11. Then a vortex line such as AB (which must always move with the fluid) will be bent over and stretched as it is convected downstream by the mean flow. The corresponding increase in the streamwise vorticity causes the transverse velocity to increase. This effect also occurs in turbulent flows over blunt bodies (for a discussion of this point and related experiments see Britter, Hunt & Mumford 1979).

Figures 5–7 show that the turbulence levels always decrease with decreasing δ/l_∞ and that the turbulence is actually suppressed below its upstream value when δ/l_∞ is sufficiently small (e.g. figure 6 shows that $\overline{u_2^2}$ is suppressed when $c = 5$ and $\delta/l_\infty < 0{\cdot}33$). This is, of course, to be expected because the blocking effect of the solid boundaries, which tends to suppress the turbulence levels, becomes negligible for the small-scale turbulence that corresponds to large values of δ/l_∞. The increased amplification with increasing δ/l_∞ also occurs because, as pointed out by Hunt (1973), the interaction between the turbulence and the mean flow, which is responsible for this amplification, increases with decreasing wavenumber.

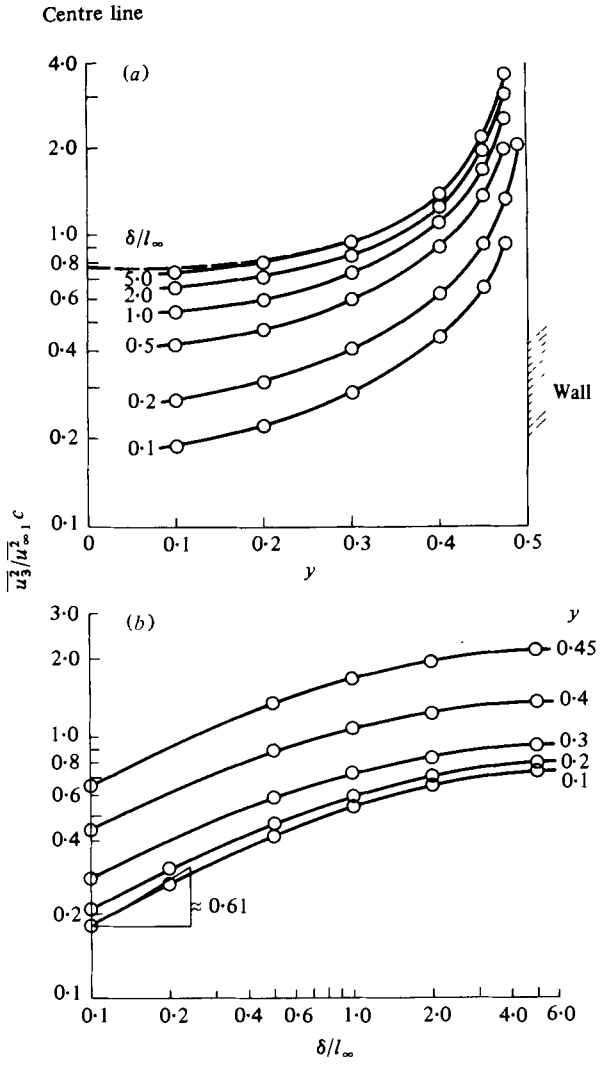

FIGURE 7. Mean-square transverse turbulence velocity ratio for large contraction ratio and arbitrary turbulence scale.

The suppression effect is reminiscent of that found by Loehrke & Nagib (1976), in their experiments on honeycomb-type turbulence control devices.

The dashed curves in figures 6 and 7 represent the asymptotic values of $\overline{u_2^2}$ and $\overline{u_3^2}$ as $\delta/l_\infty \to \infty$. They are calculated from the large-c asymptotic expansion of the classical small-scale turbulence formulas that are given by (6.16). The results are fairly close to the curve for $\delta/l_\infty = 5$, except perhaps for $\overline{u_2^2}$ near the wall, where figure 6(*b*) shows that this quantity is still increasing with δ/l_∞. In appendix C we show analytically that equations (5.13*b*, *c*) do indeed approach the results given by (6.16) as $\delta/l_\infty \to \infty$. This implies that the limit $c \to \infty$ can be interchanged with the limit $\delta/l_\infty \to \infty$ for $\overline{u_2^2}$ and $\overline{u_3^2}$.

Corresponding results are not shown for $\overline{u_1^2}$ since the curves in figure 5 are based

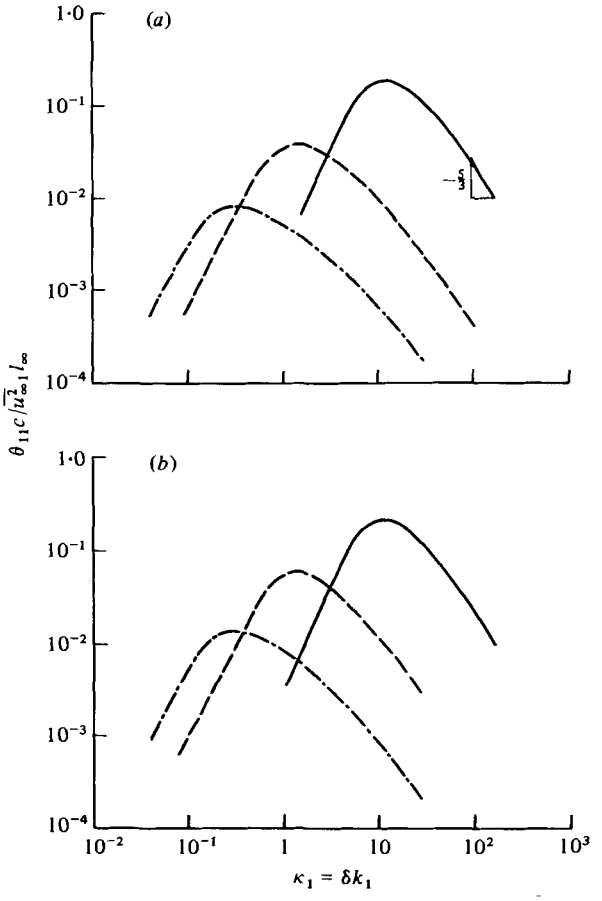

FIGURE 8. One-dimensional spectra for streamwise turbulence velocity. Large contraction ratio and arbitrary turbulence length scale. (*a*) $y = 0$; (*b*) $y = \frac{1}{4}$. ——, $\delta/l_\infty = 10$; — —, $\delta/l_\infty = 1$; — · —, $\delta/l_\infty = 0{\cdot}2$.

on the non-uniformly-valid formula (5.13*a*) with $\tilde{\gamma}$ set equal to $|\kappa_3|$ rather than on the uniformly valid result (5.10) where the second term in $\tilde{\gamma}$ is retained. In appendix C we show that this latter result does indeed agree with (6.16) in the limit as $\delta/l_\infty \to \infty$. It is therefore probable that the curves of figure 5 will be inaccurate for large δ/l_∞.

The transverse turbulence velocity $\overline{u_3^2}^{\frac{1}{2}}$ becomes infinite at the walls. This can be explained physically by noting that the upstream stagnation point produces an infinite stretching and streamwise alignment of the vortex lines that were transverse to the flow when they were far upstream (see discussion in Hunt 1973, § 5.3.3). This causes an infinite streamwise vorticity at the boundary of the downstream region which in turn produces an infinite transverse velocity. The large velocities, of course, imply that the linearized theory is invalid near the walls (see remarks about the wall layer in § 2).

The mean-square streamwise velocities remain relatively constant for large δ/l_∞ and increase with distance from the centre-line to double their initial levels when δ/l_∞ is small. For intermediate values of δ/l_∞, $\overline{u_2^2}$ remains relatively constant over most of the downstream channel and then increases rather abruptly near the walls. At large

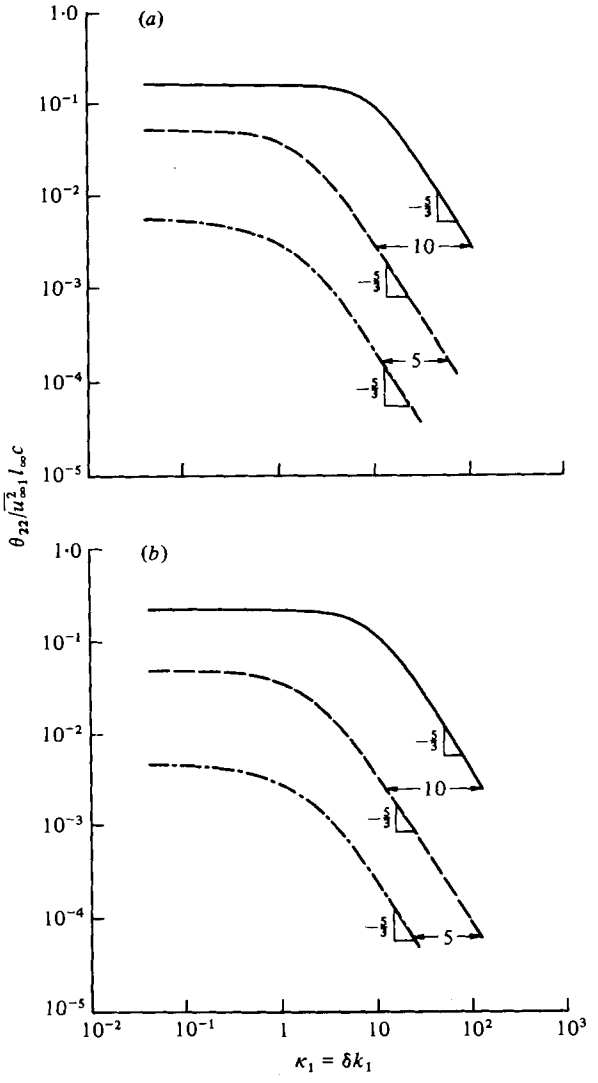

FIGURE 9. One-dimensional spectra for transverse turbulent velocities. Large contraction ratio and arbitrary turbulence length scale. (*a*) $y = 0$; (*b*) $y = \frac{1}{4}$. See figure 8 for the symbols.

values of δ/l_∞ it exhibits the rapid increase with distance from the centre-line characteristic of $\overline{u_3^2}$. (Recall that $\overline{u_2^2}$ becomes equal to $\overline{u_3^2}$ as δ/l_∞ becomes large.)

Equations (4.18) and (5.7) show that $\overline{u_2^2} = 0$ right at the wall; but $c^+ \to \infty$ as the wall is approached from within the channel, causing the u_2 intensities in figure 6 to increase without limit as the wall is approached. Physically, this occurs because the vortex lines pile up at the wall and the amplification of $\overline{u_2^2}$ by vortex stretching is able to completely counteract the wall blockage effect. Of course Δ'_+ would not tend to infinity and $\overline{u_2^2}$ would approach zero at the wall if there were no upstream stagnation point.

Equations (5.13) can be expanded for small values of δ/l_∞. The analysis is rather delicate but can readily be worked out by using Durbin's (1979) expansion technique.

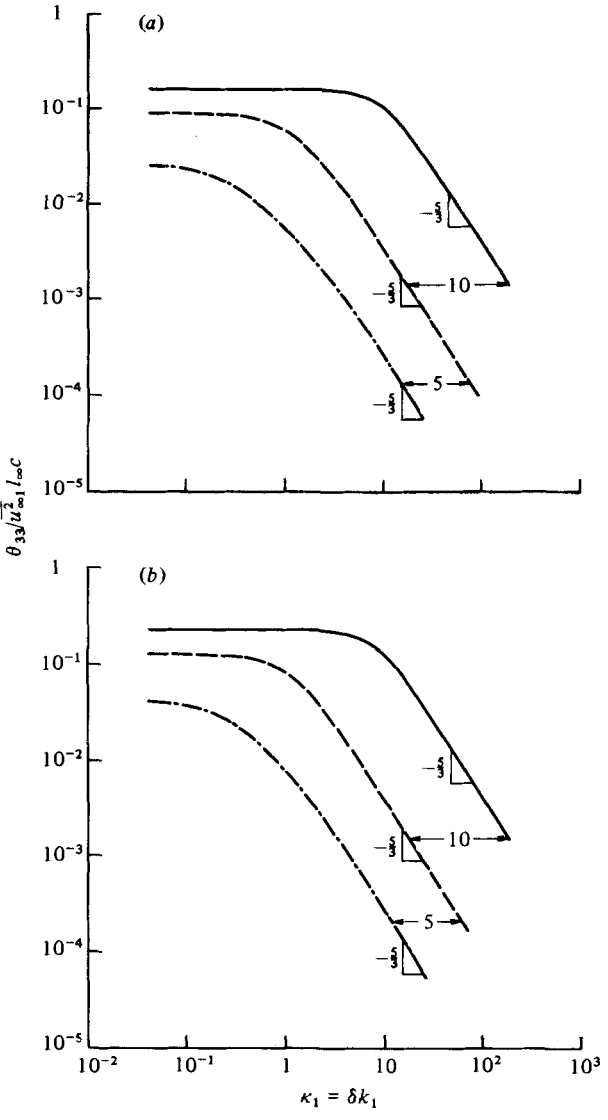

FIGURE 10. One-dimensional spectra for transverse turbulent velocities with large contraction and arbitrary turbulence scale. (*a*) $y = 0$; (*b*) $y = \frac{1}{4}$. See figure 8 for the symbols.

The result is that $\overline{u_i^2} \sim (\delta/l_\infty)^{\frac{2}{3}}$ as $\delta/l_\infty \to 0$. Britter *et al.* (1979) previously found, and verified experimentally, the more general result that $\overline{u_i^2} \sim \overline{u_i^2}(\delta/l_\infty = 0) + O((\delta/l_\infty)^{\frac{2}{3}})$ as $\delta/l_\infty \to 0, i = 1, 2, 3$. In our case $\overline{u_i^2}(\delta/l_\infty = 0) = 0$. The slopes of the curves in the second parts of figures 5 and 6 are very close to $\frac{2}{3}$ at the lowest value of δ/l_∞ but the slope of the $\overline{u_3^2}$ curve is only about 0·61 at $\delta/l_\infty = 0{\cdot}1$. However, the figure shows that the slope is still increasing with decreasing δ/l_∞.

The spectral curves plotted in figures 8–10 all have a slope of $-\frac{5}{3}$ at sufficiently large values of $k_1\delta$. This is apparent from the figures for the transverse velocity spectra but, except for the small-scale turbulence case where $\delta/l_\infty = 10$, the streamwise velocity spectra have not been carried to high enough wavenumbers to achieve this

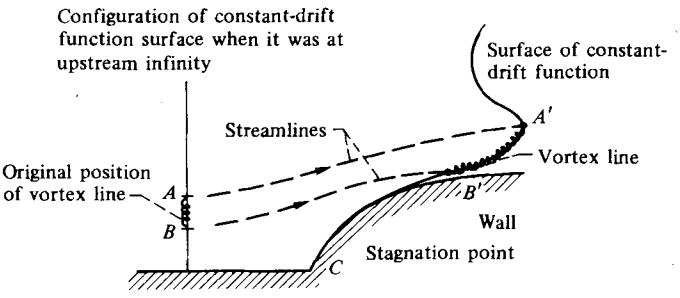

FIGURE 11. Distortion of vortex lines.

behaviour. It can also be seen that the large-wavenumber portions of the transverse velocity spectra corresponding to different values of δ/l_∞ are displaced from one another by the ratio of their δ/l_∞ values. Thus, the large-$k_1\delta$ portions of these curves would lie on top of one another if they were plotted against $k_1 l_\infty$ rather than $k_1\delta$. This is to be expected since the high-frequency portion of the spectra should behave as small-scale turbulence and not be blocked by the walls of the channel. The streamwise velocity spectrum comes fairly close to also exhibiting this behaviour but the calculations have not been carried to high enough wavenumbers to obtain an 'exact' result.

Like the turbulence velocities themselves, the one-dimensional spectra at $y = \frac{1}{4}$ are not substantially different from the corresponding centre-line spectra. Not surprisingly, the biggest differences are in the levels of the low-frequency portions of the spectra.

Figures 9 and 10 shows that Θ_{22} and Θ_{33} become identical when $\delta/l_\infty = 10$. This is also true for the large contraction-ratio expansion of the classical small-scale turbulence formulae given by (6.17*b*). In fact, the $\delta/l_\infty = 10$ curves are exactly the same as the results calculated from the small-scale turbulence formulae (6.17*b*). This of course shows that the limits $c \to \infty$ and $\delta/l_\infty \to \infty$ can also be interchanged when calculating the one-dimensional spectra of the transverse turbulence velocities.

Unlike the transverse velocity spectra, the streamwise velocity spectra tend to zero as $\delta k_1 \to 0$. In the asymptotic limit process it was assumed that c would be large enough to ensure that $c\delta k_1$ would also be large. The expansion therefore becomes invalid as $k_1 \to 0$, where the neglected terms of $O(c^{-1})$ become important. However, the behaviour of the classical small-scale turbulence spectra, for arbitrary c given by (6.17*c*), suggests the manner in which $\Theta_{11}(0)$ should tend to zero as $c \to \infty$. We have not included the calculations of the small-scale turbulence spectra for arbitrary c that would serve to illustrate its development from the undistorted spectrum $\Theta_{11}^{\infty}(k_1)$ to its large-c asymptotes given by (6.17*a*) and (6.17*b*); but its behaviour is somewhat analogous to that shown in Hunt's (1973) figure 11.

We could have made the present results uniformly valid in wavenumber space by retaining higher-order terms in c^{-1} but the linearized analysis itself may be inadequate for calculating the large contraction-ratio limit of the streamwise velocity correlations and their spectra. This is because the energy in the transverse velocity components of the turbulence increases while that in the streamwise component decreases. Then while the energy transfer between the turbulence wavenumber components, which is

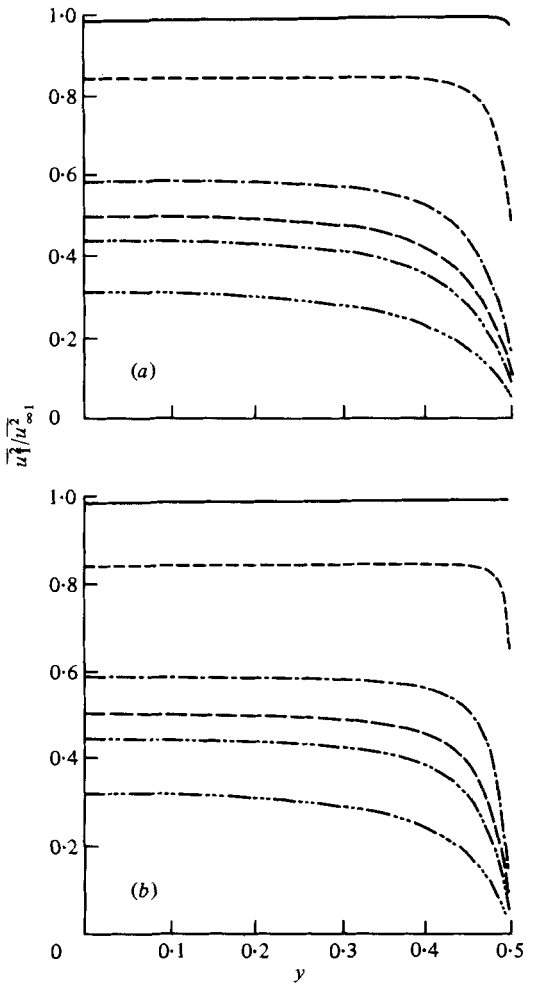

FIGURE 12. Mean-square streamwise turbulence velocity ratio for small-scale turbulence and arbitrary contraction ratio. (*a*) Internal channel flow. (*b*) Inlet flow. ——, $c = 1{\cdot}02$; - - - -, $c = 1{\cdot}25$; — · —, $c = 2$; — —, $c = 2{\cdot}5$; - - - -, $c = 3$; - - - - -, $c = 5$.

neglected in linear theory, represents only a small energy drain relative to the transverse velocity components it can be a significant fraction of the energy in the streamwise components.

7.2. *Small-scale turbulence: quasi-homogeneous limit*

Figures 12–14 are plots of the mean-square turbulence velocity ratios for the case where the turbulence spatial scale is small but the contraction ratio of the flow is arbitrary. The calculations are based on equations (6.13) and the drift function derivatives are calculated from the equations given in appendices A and B. The first part of each figure corresponds to the internal flow depicted in figure 15 and described in appendix A. The second part corresponds to the two-dimensional inlet flow depicted in figure 16 and described in appendix B. The results for these two flows are quite similar and are appreciably different in magnitude only near the wall.

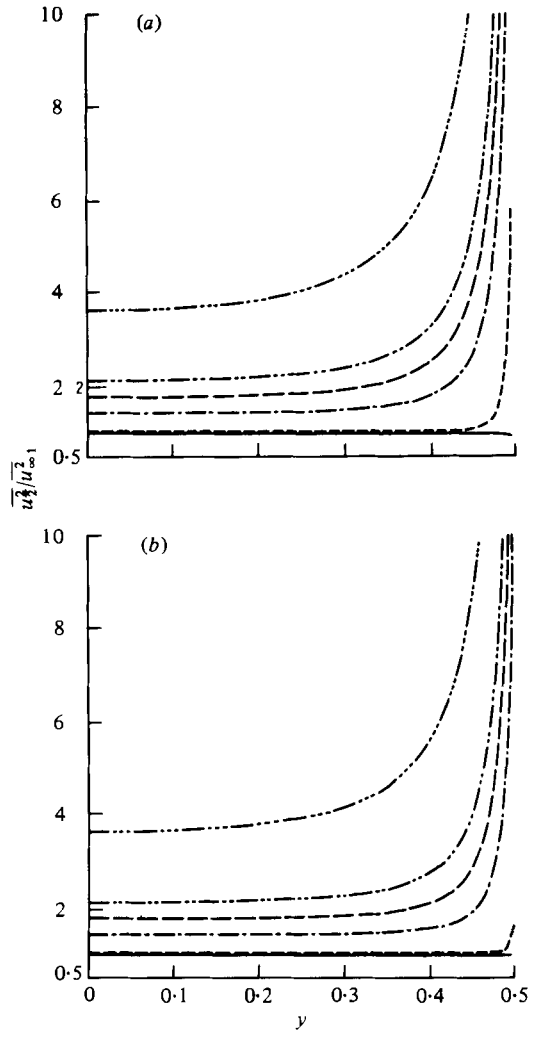

FIGURE 13. Mean-square transverse turbulent velocity ratio for small-scale turbulence and arbitrary contraction ratio. (*a*) Internal channel flow. (*b*) Inlet flow. See figure 12 for the symbols.

The curves agree with the asymptotic expansions (6.18) for small values of the contraction ratio and with the asymptotic expansions (6.16) for large values of the contraction ratio.

Equations (6.18) imply that the $\overline{u_i^2}$ will be independent of position y when $c \lesssim 2$ and the figures show that this occurs in the main part of the channel. The expansions (6.18) are invalid near the wall where the $\overline{u_i^2}$ are nonconstant. In fact, $c^\dagger = c(1+[\Delta'_+]^2)^{\frac{1}{2}}$ will be large and the large contraction-ratio expansion (6.16) will apply when

$$\tfrac{1}{2} - |y| \ll c - 1.$$

The figures show that the results for different contraction ratio are indeed similar near the wall.

Equations (6.16) imply that $\overline{u_2^2}$ and $\overline{u_3^2}$ should become equal when $c^\dagger$ becomes large

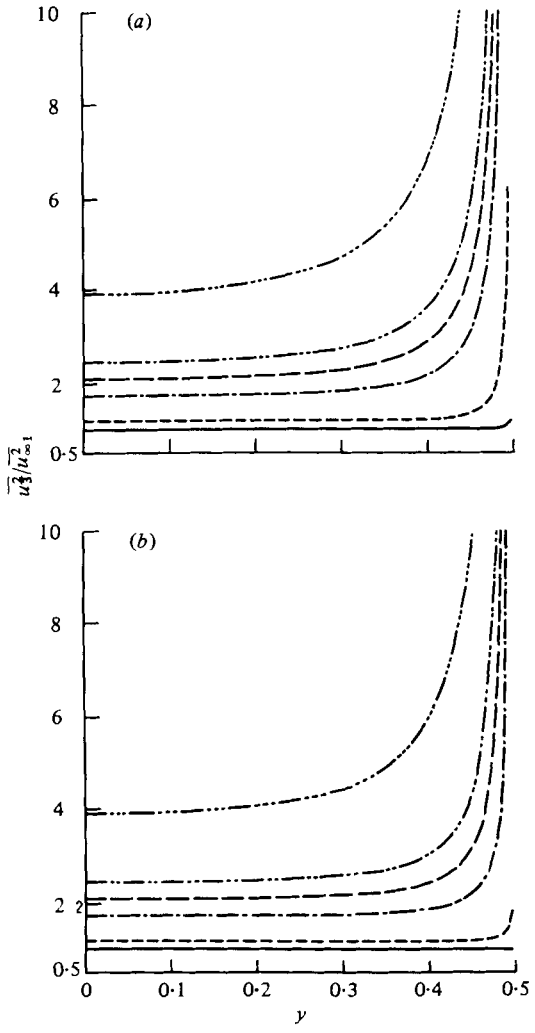

FIGURE 14. Mean-square transverse velocity ratios for small-scale turbulence and arbitrary contraction ratio. (*a*) Internal channel flow. (*b*) Inlet flow. See figure 12 for the symbols.

and figures 12 and 13 show that $\overline{u_2^2}$ and $\overline{u_3^2}$ differ mainly when c is small and y is not too close to the wall.

It can be seen that the amplification of the transverse velocity components and the suppression of the streamwise velocity components increases at all points of the channel when the contraction ratio is increased. The effect is always greatest near the walls, and the size of the wall region where this enhanced effect occurs always increases with contraction ratio. For small contractions the turbulence is nearly unaffected by the contraction over the major portion of the channel.

Since no boundary conditions are applied in the small-scale limit we can take any mean streamline to be the wall. Then for continuous internal flows this streamline can be chosen to make Δ'_+ non-singular at the wall. We can then account for surface-blockage effects by appending a wall layer of thickness $O(l_\infty/\delta)$ and imposing a no-flux boundary condition across this layer. The analysis of such a layer was worked

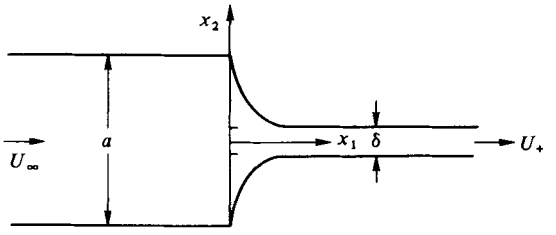

FIGURE 15. Geometry of the internal contracting flow.

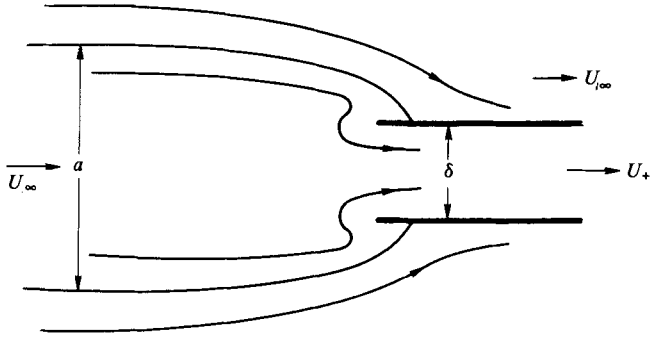

FIGURE 16. Geometry of two-dimensional inlet flow.

out by Hunt & Graham (1978). Let the turbulence intensity at a point one integral scale away from the wall be $\overline{u_{iL}^2}$; $i = 1, 2, 3$ and the corresponding distance from the wall be Y, then the result of this analysis can be written as

$$\left.\begin{aligned} \overline{u_2^2} &\to O((Y/l_\infty)^{\frac{2}{3}}) \\ \overline{u_1^2}+\overline{u_3^2} &\to \overline{u_{iL}^2}+\overline{u_{2L}^2}+\overline{u_{3L}^2} \end{aligned}\right\} \quad \text{as} \quad Y \to 0.$$

8. Concluding remarks

The results obtained by Batchelor & Proudman and Ribner & Tucker for the amplification of turbulence by a contracting stream have been extended to include the effects of finite turbulence length scale. The calculations show that the blocking effect of the solid surfaces, which only occurs near the walls when the turbulence scale is small relative to the downstream duct width, will, at intermediate scales, greatly limit the amount of amplification of the turbulence that the contraction can produce and in some cases will even cause the turbulence to be suppressed.

The present analysis can be extended to include compressibility effects for cases where it is possible to separate out the acoustic field from the turbulence. The techniques developed herein can also be used to predict the effects of finite turbulence length scale on entropy-generated turbulence.

The authors would like to thank Dr Theodore Fessler for carrying out the numerical computations and Dr J. C. R. Hunt and Dr H. M. Nagib for their helpful comments.

Appendix A. Calculation of drift function for a converging channel

The incompressible flow through a two-dimensional converging passage can be modelled by superimposing a uniform flow on an infinite row of point sources distributed uniformly along the x_2 axis (see figure 15). This produces a uniform velocity field at both upstream and downstream infinity.

The complex potential $W = \Phi + i\Psi$ is given by

$$W = \frac{U_\infty + U_+}{2} Z + \frac{U_+ - U_\infty}{2} \frac{a}{\pi} \left[\ln \sinh \pi \left(\frac{Z}{a} + \frac{i}{2} \right) - \frac{i\pi}{2} \right], \tag{A 1}$$

where $Z = x_1 + ix_2$. Hence the complex conjugate velocity $\zeta = U_1 - iU_2$ is given by

$$\zeta = \frac{dW}{dZ} = \frac{U_+ + U_\infty}{2} + \frac{U_+ - U_\infty}{2 \tanh \pi \left(\frac{Z}{a} + \frac{i}{2} \right)}. \tag{A 2}$$

Taking the imaginary part of (A 1) we obtain

$$\Psi = \frac{U_+ + U_\infty}{2} x_2 - \frac{U_+ - U_\infty}{2} \frac{a}{\pi} \left\{ \tan^{-1} \left[\frac{\cot (\pi x_2/a)}{\tanh (\pi x_1/a)} \right] + \frac{\pi}{2} \right\}. \tag{A 3}$$

Then
$$\Psi \to U_+ x_2 \quad \text{as} \quad x_1 \to +\infty. \tag{A 4}$$

Solving (A 3) for x_1, we find

$$x_1 = \frac{a}{2\pi} \ln \frac{\sin \frac{2\pi}{a} \left(\frac{\Psi - x_2 U_\infty}{U_+ - U_\infty} \right)}{\sin \frac{2\pi}{a} \left(\frac{\Psi - x_2 U_+}{U_+ - U_\infty} \right)}, \tag{A 5}$$

$$\cosh \frac{2\pi x_1}{a} = -\frac{1}{2} \left[2 \cos \left(\frac{2\pi x_2}{a} \right) + \frac{\sin \left(\frac{2\pi x_2}{a} \right)}{\tan \frac{2\pi}{a} \left(\frac{\Psi - U_+ x_2}{U_+ - U_\infty} \right)} - \frac{\sin \left(\frac{2\pi x_2}{a} \right)}{\tan \frac{2\pi}{a} \left(\frac{\Psi - x_2 U_\infty}{U_+ - U_\infty} \right)} \right]. \tag{A 6}$$

Taking the imaginary part of (A 2), we find

$$U_2 = -\frac{U_+ - U_\infty}{2} \frac{\sin (2\pi x_2/a)}{\cosh (2\pi x_1/a) + \cos (2\pi x_2/a)}.$$

Hence it follows from (A 5) and (A 6) that

$$\begin{aligned} \int \frac{dx_2}{U_2[x_1(x_2, \Psi), x_2]} &= \frac{a}{2\pi} \left[\frac{1}{U_\infty} \ln \sin \frac{2\pi}{a} \left(\frac{\Psi - x_2 U_\infty}{U_+ - U_\infty} \right) - \frac{1}{U_+} \ln \sin \frac{2\pi}{a} \left(\frac{\Psi - x_2 U_+}{U_+ - U_\infty} \right) \right] \\ &= \frac{x_1(x_2, \Psi)}{U_\infty} + \frac{a}{2\pi} \left(\frac{1}{U_\infty} - \frac{1}{U_+} \right) \ln \sin \frac{2\pi}{a} \left(\frac{\Psi - x_2 U_+}{U_+ - U_\infty} \right). \end{aligned}$$

Then since
$$\frac{dx_2}{U_2(x_1(x_2, \Psi), x_2)} = \frac{dx_1}{U_1(x_1, x_2(\Psi, x_1))}$$

it follows from (2.8) and (4.3) that

$$\frac{X_1}{U_\infty} = \frac{x_1(x_2,\Psi)}{U_\infty} + \frac{a}{2\pi}\left(\frac{1}{U_\infty}-\frac{1}{U_+}\right)\ln\left[\frac{\sin\frac{2\pi}{a}\left(\frac{\Psi - x_2U_+}{U_+-U_\infty}\right)}{\sin\frac{2\pi}{a}\left(\frac{\Psi}{U_\infty}\right)}\right]$$

$$= \frac{x_1(x_2,\Psi)}{U_+} + \frac{a}{2\pi}\left(\frac{1}{U_\infty}-\frac{1}{U_+}\right)\ln\left[\frac{\sin\frac{2\pi}{a}\left(\frac{\Psi - x_2U_\infty}{U_+-U_\infty}\right)}{\sin\frac{2\pi}{a}\left(\frac{\Psi}{U_\infty}\right)}\right].$$

Hence it follows from (A 4), (4.5), (4.7), and (4.17) that

$$\Delta_+(y) = \frac{1}{2\pi}\left(\frac{1}{c}-1\right)\left\{\ln\left[\sin(2\pi y)\right] - \ln\left[\sin\left(\frac{2\pi y}{c}\right)\right]\right\} + \text{constant}. \tag{A 7}$$

Then
$$\Delta_+(y) = -\frac{1}{2\pi}\{\ln\left[\sin(2\pi y)\right] - \ln y\} + O(c^{-1}) \quad \text{as} \quad c\to\infty,$$

$$\Delta'_+(\eta) = \frac{1}{2\pi\eta} - \frac{1}{\tan 2\pi\eta} + O(c^{-1}) \quad \text{as} \quad c\to\infty, \tag{A 8}$$

and
$$\Delta''_+(\eta_0) = 2\pi\left[\frac{1}{\sin^2 2\pi\eta_0} - \frac{1}{(2\pi\eta_0)^2}\right] + O(c^{-1}) \quad \text{as} \quad c\to\infty, \tag{A 9}$$

$$\Delta_+(y) = \frac{y(c-1)^2}{\tan 2\pi y} + O[(c-1)^3] \quad \text{as} \quad c\to 1. \tag{A 10}$$

Appendix B. Calculation of drift function for two-dimensional inlet flow

The incompressible flow into a two-dimensional inlet can be calculated by superimposing a uniform flow onto the solution for the flow into a two-dimensional channel that is at rest relative to the fluid at infinity (see figure 16).

The problem with zero mean flow at infinity is discussed by Lamb (1932). The streamlines are depicted on his page 74. When $c\to\infty$ the formulas obtained below will reduce to this result. Unlike the case considered in appendix A, the flow into the channel produces a sink flow far upstream which violates the criterion for the validity of (2.6) that is set forth just above that equation. However, this formula is valid for all three-dimensional flows and we shall show below that the formula which we obtain is the correct 'inner expansion' of the drift function for a three-dimensional channel of large aspect ratio. The complex potential $W = \Phi + i\Psi$ is given by

$$W = ZU_+ + e^{-2\pi(W-U_\infty Z)/(U_+-U_\infty)\delta}, \tag{B 1}$$

where $Z = x_1 + ix_2$. Hence the complex conjugate velocity $\zeta = U_1 - iU_2$ is given by

$$\zeta = \frac{U_+ + AU_\infty e^{-A(W-U_\infty Z)}}{1 + A\,e^{-A(W-U_\infty Z)}}, \tag{B 2}$$

where
$$A \equiv 2\pi/\delta(U_+ - U_\infty). \tag{B 3}$$

Taking the real and imaginary parts of (B 1), we obtain

$$\left.\begin{aligned} x_1U_+ &= \Phi - e^{-A(\Phi - U_\infty x_1)}\cos A(\Psi - U_\infty x_2),\\ x_2U_+ &= \Psi + e^{-A(\Phi - U_\infty x_1)}\sin A(\Psi - U_\infty x_2).\end{aligned}\right\} \tag{B 4}$$

Then eliminating Φ

$$A(U_+ - U_\infty)x_1 = -\ln\left[\frac{x_2U_+ - \Psi}{\sin A(\Psi - U_\infty x_2)}\right] - \frac{A(x_2U_+ - \Psi)}{\tan A(\Psi - U_\infty x_2)}. \tag{B 5}$$

Taking the imaginary part of (B 2) and using (B 5) to eliminate x_1, we find

$$U_2 = \frac{A(U_\infty - U_+)(x_2U_+ - \Psi)}{1 + 2A(x_2U_+ - \Psi)/\tan A(\Psi - U_\infty x_2) + A^2(x_2U_+ - \Psi)^2/\sin^2 A(\Psi - U_\infty x_2)}.$$

Hence from (B 5) and the second (B 4)

$$\int \frac{dx_2}{U_2[x_1(x_2, \Psi), x_2]} = \frac{1}{U_\infty - U_+}\left\{\frac{1}{A}\left(\frac{1}{U_+} - \frac{1}{U_\infty}\right)\ln(x_2U_+ - \Psi)\right.$$
$$+ \frac{1}{AU_\infty}\left(\frac{U_+}{U_\infty} - 1\right)\ln\sin A(\Psi - U_\infty x_2) + \frac{1}{AU_\infty}\ln\left[\frac{x_2U_+ - \Psi}{\sin A(\Psi - U_\infty x_2)}\right]$$
$$\left. + \frac{x_2U_+ - \Psi}{U_\infty \tan A(\Psi - U_\infty x_2)}\right\} = 2\frac{x_1(x_2, \Psi)}{U_\infty} - \frac{\Phi(x_2, \Psi)}{U_\infty^2} + \frac{1}{AU_\infty}\left(\frac{1}{U_+} - \frac{1}{U_\infty}\right)\ln(x_2U_+ - \Psi).$$

Now in this case it is impossible to define X_1 by (2.8) since the integral will not converge. But since

$$dx_2/U_2(x_1(x_2, \Psi), x_2) = dx_1/U_1(x_1, x_2(\Psi, x_1))$$

we find

$$\int_{-\infty}^{x_1}\left[\frac{1}{U_1(x_1, x_2(\Psi, x_1))} - \frac{2}{U_\infty} + \frac{U_1(x_1, x_2(\Psi, x_1))}{U_\infty^2}\right]dx_1 + \frac{1}{U_\infty}\left[2x_1 - \frac{\Phi(x_1, x_2(x_1, \Psi))}{U_\infty}\right]$$
$$= \frac{2x_1(x_2, \Psi)}{U_\infty} - \frac{\Phi(x_1(x_2, \Psi), x_2)}{U_\infty^2} + \frac{1}{AU_\infty}\left(\frac{1}{U_+} - \frac{1}{U_\infty}\right)\ln\left[\frac{x_2U_+ - \Psi}{\Psi\left(\frac{U_+}{U_\infty} - 1\right)}\right].$$

The integral will now converge but the left-hand side of this equation will not approach x_1/U_∞ as $x_1 \to -\infty$ since $\Phi - U_\infty x_1$ is logarithmically infinite there. This is because the flow is two-dimensional. However, we can think of this solution as a near-field approximation to the solution for a three-dimensional channel of large aspect ratio. In the three-dimensional solution $\Phi - U_\infty x_1$ will approach zero and we can therefore identify the left-hand side of this result with X_1/U_∞.

Then since it follows from (B 4) and (B 5) that

$$-A(U_+ - U_\infty)x_1 \to \ln\left[\frac{x_2U_+ - \Psi}{\sin A(\Psi - U_\infty x_2)}\right], \quad \Phi \to U_+x_1 \quad \text{as} \quad x_1 \to -\infty$$

we find

$$\frac{X_1}{U_\infty} \to \frac{x_1}{U_+} + \frac{1}{AU_\infty}\left(\frac{1}{U_+} - \frac{1}{U_\infty}\right)\ln\left[\frac{\sin A(\Psi - U_\infty x_2)}{\Psi(U_+/U_\infty - 1)}\right].$$

Hence it follows from (4.5), (4.7) and (4.17) that

$$\Delta_+(y) = -\frac{1}{2\pi}\left(1 - \frac{1}{c}\right)^2[\ln\sin 2\pi y - \ln y].$$

Notice that this becomes identical to (A 7) when $c \to \infty$.

Appendix C. Limit of large contraction-ratio solution

In order to calculate $\lim_{\sigma\to 0}\ (\lim_{c\to\infty} \overline{u_1^2})$ we must retain the κ_1/c term in

$$\tilde{\gamma} \equiv (\kappa_3^2 + (\kappa_1/c)^2)^{\frac{1}{2}}.$$

Then if, in accordance with (4.23), we let

$$\tilde{\gamma} = \left\{\kappa_3^2 + \left[\frac{\kappa_0}{c\{1+[\Delta'_+(\eta_0)]^2\}^{\frac{1}{2}}}\right]^2\right\}^{\frac{1}{2}} \to \infty,$$

$$[\tilde{\gamma}\mathscr{K}_1^-(y\mid\eta_0)]^2 \sim [\mathscr{K}_2^+(y\mid\eta_0)]^2 \sim \tfrac{1}{4}e^{-2\tilde{\gamma}|y-\eta_0|}.$$

Since this quantity is effectively equal to zero except when $\eta_0 = y$ it follows that

$$\begin{aligned}\int_{-\frac{1}{2}}^{\frac{1}{2}} \frac{H(\kappa, -\tan^{-1}\Delta'_+(\eta_0),\phi)}{\{1+[\Delta'_+(\eta_0)]^2\}^{\frac{1}{2}}}[\mathscr{K}_2^+(y\mid\eta_0)]^2\,d\eta_0 &\sim \frac{H(\kappa,-\tan^{-1}\Delta'_+(y),\phi)}{4\{1+[\Delta'_+(y)]^2\}^{\frac{1}{2}}}\int_{-\frac{1}{2}}^{\frac{1}{2}} e^{-2\tilde{\gamma}|y-\eta_0|}\,d\eta_0\\ &\sim \frac{H(\kappa,-\tan^{-1}\Delta'_+(y),\phi)}{4\{1+[\Delta'_+(y)]^2\}^{\frac{1}{2}}\left\{\kappa_3^2+\left[\frac{\kappa_0}{c\{1+[\Delta'_+(y)]^2\}^{\frac{1}{2}}}\right]^2\right\}^{\frac{1}{2}}}\frac{1}{2}\int_{-\frac{1}{2}}^{\frac{1}{2}} e^{-|x|}\,dx\\ &= \frac{H(\kappa,-\tan^{-1}\Delta'_+(y),\phi)}{4\{1+[\Delta'_+(y)]^2\}^{\frac{1}{2}}\left\{\kappa_3^2+\left[\frac{\kappa_0}{c\{1+[\Delta'_+(y)]^2\}^{\frac{1}{2}}}\right]^2\right\}^{\frac{1}{2}}}, \qquad \text{(C 1)}\end{aligned}$$

where ϕ is the polar angle $\tan^{-1}(\kappa_0/\kappa_3)$. Similarly

$$\begin{aligned}\int_{-\frac{1}{2}}^{\frac{1}{2}} H(\kappa,-\tan^{-1}\Delta'_+(\eta_0),\phi)\{1+[\Delta'_+(\eta_0)]^2\}^{\frac{1}{2}}[\tilde{\gamma}^2\mathscr{K}_1^-(y\mid\eta_0)]^2\,d\eta_0 &\sim \frac{H(\kappa,-\tan^{-1}\Delta'_+(y),\phi)}{4}\{1+[\Delta'_+(y)]^2\}^{\frac{1}{2}}\left\{\kappa_3^2+\left[\frac{\kappa_0}{c\{1+[\Delta'_+(y)]^2\}^{\frac{1}{2}}}\right]^2\right\}^{\frac{1}{2}}, \qquad \text{(C 2)}\\ \int_{-\frac{1}{2}}^{\frac{1}{2}} H(\kappa,-\tan^{-1}\Delta'_+(\eta_0),\phi)\{1+[\Delta'_+(\eta_0)]^2\}^{\frac{1}{2}}[\mathscr{K}_2^+(y\mid\eta_0)]^2\,d\eta_0 &\sim \frac{H(\kappa,-\tan^{-1}\Delta'_+(y),\phi)}{4\left\{\kappa_3^2+\left[\frac{\kappa_0}{c\{1+[\Delta'_+(y)]^2\}^{\frac{1}{2}}}\right]^2\right\}^{\frac{1}{2}}}\{1+[\Delta'_+(y)]^2\}^{\frac{1}{2}}. \qquad \text{(C 3)}\end{aligned}$$

Now if we were to omit the second term in

$$\left\{\kappa_3^2+\left[\frac{\kappa_0}{c\{1+[\Delta'_+(y)]^2\}^{\frac{1}{2}}}\right]^2\right\}^{\frac{1}{2}}$$

when c is large the integral in the first of equation (5.10) would become infinite. Therefore in order to obtain a formula that gives the correct behaviour for large but not infinite c we must retain this term and let $c\to\infty$ after the integration is carried out. Thus when the upstream turbulence is isotropic H is given by (5.12) and is therefore independent of its second argument $-\tan^{-1}\Delta'_+(y)$. Then since

$$\kappa_0\,d\kappa_0\,d\kappa_3 = \sin\phi\kappa^2\,d\kappa\,d\phi, \quad \kappa_0 = \kappa\sin\phi, \quad \kappa_3 = \kappa\cos\phi,$$

it follows from the first equation (5.10) that

$$\overline{u_1^2} \sim \frac{1}{4c\{1+[\Delta'_+(y)]^2\}^{\frac{1}{2}}}\int_0^\infty E(k)\,dk\int_0^\infty \frac{\sin^2\phi}{\{\cos^2\phi+\lambda^2\sin^2\phi\}^{\frac{1}{2}}}\,d\phi,$$

where $$\lambda^2 \equiv \frac{1}{c^2(1+[\Delta'_+(y)]^2)}.$$

Then since (Abramowitz & Stegun 1964, p. 559)

$$\int_0^\pi \frac{\sin^2\phi}{\{\cos^2\phi+\lambda^2\sin^2\phi\}^{\frac{1}{2}}} = \frac{\pi}{2}F(\tfrac{3}{2},\tfrac{1}{2};2;1-\lambda)$$
$$\to 2\psi(1)-\psi(\tfrac{3}{2})-\psi(\tfrac{1}{2})-\lambda^2 = 2[\ln(4/\lambda)-1] \quad \text{as} \quad \lambda\to 0,$$

where F is the hypergeometric function in the usual notation. Then since (Batchelor 1953, p. 49)

$$\int_0^\infty E(k)\,dk = \tfrac{3}{2}$$

it follows that

$$u_1^2 \sim \frac{3}{4c\{1+[\Delta'_+(y)]^2\}^{\frac{1}{2}}}[\ln(4c\{1+[\Delta'_+(y)]^2\}^{\frac{1}{2}})-1] \quad \text{as} \quad l_\infty\to 0, \quad c\to\infty. \tag{C 4}$$

On the other hand the integrals in the second and third equations (5.10) will exist if we put $c=\infty$ in

$$\left\{\kappa_3^2+\left[\frac{\kappa_0}{c\{1+[\Delta_+(y)]^2\}^{\frac{1}{2}}}\right]^2\right\}^{\frac{1}{2}}.$$

Then for initially isotropic turbulence we find in a similar way that

$$\overline{u_2^2}, \overline{u_3^2} \sim \tfrac{3}{4}c\{1+[\Delta'_+(y)]^2\}^{\frac{1}{2}}. \tag{C 5}$$

Appendix D. Transformation of small-scale turbulence transfer coefficients into the Batchelor–Proudman form

Since T_{lj} has determinant one, it follows from the Laplace development of this determinant that

$$\epsilon_{mnj} = \epsilon_{qpl}T_{qm}T_{pn}T_{lj}.$$

Then since $$\tilde{\chi}_i = T_{ij}\kappa_j,$$

and $$T_{lj}T^{-1}_{ji} = \delta_{li},$$

it follows that $$\kappa_n\epsilon_{mnj}T^{-1}_{mk} = \epsilon_{kpl}\tilde{\chi}_p T_{lj}.$$

Substituting into (6.3) yields

$$M_{ij} = \frac{\kappa_n\tilde{\chi}_r\epsilon_{kri}\epsilon_{mnj}T^{-1}_{mk}}{\tilde{\chi}^2}, \tag{D 1}$$

which coincides with the result used by Batchelor & Proudman (1954).

REFERENCES

Abramowitz, M. & Stegun, I. 1964 *Handbook of Mathematical Functions.* Washington: National Bureau of Standards.

Batchelor, G. K. 1953 *The Theory of Homogeneous Turbulence.* Cambridge University Press.

Batchelor, G. K. 1967 *An Introduction to Fluid Mechanics.* Cambridge University Press.

Batchelor, G. K. & Proudman, I. 1954 The effect of rapid distortion of a fluid in turbulent motion. *Quart. J. Mech. Appl. Math.* **7**, 83.

BRITTER, R. E., HUNT, J. C. R. & MUMFORD, J. C. 1979 The distortion of turbulence by a circular cylinder. *J. Fluid Mech.* **92**, 269.

DARWIN, C. G. 1953 A note on hydrodynamics. *Proc. Camb. Phil. Soc.* **49**, 342.

DURBIN, P. 1979 Ph.D. thesis, Cambridge University. (See also *J. Inst. Math. Appl.* (1979) **23**, 181).

ERDÉLYI, A. 1956 *Asymptotic Expansion*, p. 51. Dover.

GOLDSTEIN, M. E. 1976 *Aeroacoustics*. McGraw-Hill.

GOLDSTEIN, M. E. 1978 Unsteady vortical and entropic distortions of potential flows around arbitrary obstacles. *J. Fluid Mech.* **89**, 433.

GOLDSTEIN, M. E. 1979 Turbulence generated by the interaction of entropy fluctuations with non-uniform mean flows. *J. Fluid Mech.* **93**, 209.

HINZE, J. O. 1959 *Turbulence*. McGraw-Hill.

HUNT, J. C. R. 1973 A theory of turbulent flow round two-dimensional bluff bodies. *J. Fluid Mech.* **61**, 625.

HUNT, J. C. R. & GRAHAM, J. M. R. 1978 Free-stream turbulence near plane boundaries. *J. Fluid Mech.* **89**, 209.

KOVASZNAY, L. S. G. 1953 Turbulence in supersonic flow. *J. Aero. Sci.* **20**, 657.

LAMB, H. 1932 *Hydrodynamics*. Cambridge University Press.

LIGHTHILL, M. J. 1956 Drift. *J. Fluid Mech.* **1**, 31.

LOEHRKE, R. E. & NAGIB, H. M. 1976 Control of free-stream turbulence by means of honeycombs: A balance between suppression and generalism. *Trans. A.S.M.E.* I, *J. Fluids Engng* **98**, 342.

PHILLIPS, O. M. 1955 The irrotational motion outside of a free boundary layer. *Proc. Camb. Phil. Soc.* **51**, 220.

RIBNER, H. S. & TUCKER, M. 1953 Spectrum of turbulence in a contracting stream. *N.A.C.A. Rep.* 1113.

TAYLOR, G. I. 1935 Turbulence in a contracting stream. *Z. angew. Math. Mech.* **15**, 91.

TOWNSEND, A. A. 1976 *The Structure of Turbulent Shear Flow*. Cambridge University Press.

TUCKER, H. J. & REYNOLDS, A. J. 1968 The distortion of turbulence by irrotational plane strain. *J. Fluid Mech.* **32**, 657.